

FINAL PUBLISHABLE REPORT

Grant Agreement number 14IND02
 Project short name PlanarCal
 Project full title Microwave measurements for planar circuits and components

Project start date and duration:		01 October 2015, 36 months
Coordinator: Dr. Uwe Arz, PTB		Tel: +49 531 592 2297
Project website address: https://planarcal.ptb.de		E-mail: uwe.arz@ptb.de
Internal Funded Partners:	External Funded Partners:	Unfunded Partners:
1 PTB, Germany	4 FAU, Germany	10 RF360, Germany
2 NPL, United Kingdom	5 FhG, Germany	11 METAS, Switzerland
3 VSL, Netherlands	6 FVB, Germany	12 R&S, Germany
	7 TU Delft, Netherlands	
	8 ULE, United Kingdom	
	9 Univ-Lille1, France	



TABLE OF CONTENTS

1	Overview	3
2	Need	3
3	Objectives	3
4	Results	4
5	Impact	27
6	List of publications	30
7	Contact details	32

1 Overview

The overall aim of this project was to enable the traceable measurement and electrical characterisation of scattering parameters (S-parameters) of integrated planar circuits and components from radio-frequency (RF) to sub-mm frequencies. This project developed an extensive set of measurement capabilities ranging from nanodevice characterisation and dedicated calibration software to traceable planar S-parameter measurements for frequencies up to 110 GHz. A calibration service for traceable on-wafer measurements is currently put in place at PTB, and first steps towards an Institute of Electrical and Electronics Engineers (IEEE) standard for on-wafer microwave measurements have been made. The results of this project enable manufacturers of planar microwave circuits and components to offer assured products with defensible specifications which are supported for the first time through on-wafer measurement traceability chains.

2 Need

Although on-wafer high-frequency measurements already had an economic impact on chip fabrication costs, industrial assurance and traceability were not established before this project. Boundary conditions of the measurement system setup and parasitic modes were often not sufficiently considered, leading to inconsistent results. This project has used the most advanced vector network analysers (VNAs) that are currently available together with state-of-the-art numerical simulation techniques to fully capture all relevant effects. At the end of this project, industry has been provided with methods to perform reliable on-wafer scattering-parameter (S-parameter - an electrical description of the transmission/reflection behaviour of a device at higher frequencies) measurements down to mm wavelengths.

Using a certain transmission-line system for calibration purposes in planar circuits requires adequate knowledge of its high-frequency properties. Until recently, relatively simple line models have been used describing these properties with sufficient accuracy for circuit designs in the frequency range of some tens of GHz. With increasing frequency and with the ongoing developments in semiconductor technologies more and more parasitic effects need to be taken into account. This includes, particularly, crosstalk due to field coupling and substrate modes, radiation into the environment, and increased losses due to the microscopic structure of the conductor surfaces.

High-frequency on-wafer science, engineering and metrology are underpinning technologies for almost all applications that employ micro- and nano-electronics. Integrated circuits operated in the microwave and mm wave frequency range are in widespread use, in applications ranging from mobile communications to sensors. The ubiquitous presence of wireless data transmission that we are used to would not be possible without them. However, the demands for higher data rates, the growing number of services to be covered, and the development of high-resolution (radar) imaging have been continuously pushing up the frequency of operation. 60 GHz short-range high-data rate communications and automotive radar at 77 GHz are examples of important applications at higher frequencies which have recently been deployed. Beyond this, various applications for imaging, material testing, and ultra-broadband wireless links are envisaged above 100 GHz. These needs will be intensified by the Internet of Things (IoT) initiative of the European Commission (EC), which strongly relies on wireless networks and wireless sensor functions.

3 Objectives

The aim of the project was to enable industry to characterise integrated planar circuits and components for ultimate use in high-speed and microwave applications with known measurement uncertainties.

The specific scientific and technical objectives of the project were to:

- Establish traceability of planar scattering parameter measurements on reference calibration substrates. The aim was to provide the lowest possible uncertainties for scattering parameter measurements of devices embedded on the same wafer, and to quantify the uncertainties. Candidates for these calibrations, such as airline-like interconnects in membrane technology and substrates such as GaAs which allow for comparisons to electro-optic waveform metrology, have been evaluated.
- Transfer uncertainties to calibration standards in conventional technology to be used in industry. This addressed the difficulty of moving between different substrate materials and different planar waveguide

types. Residual errors of the calibration have been quantified with regard to the selected calibration algorithms and the influences of probe geometry and technology.

- Improve planar transmission lines models accounting for surface roughness and radiation losses. This not only helped develop reliable uncertainty budgets for planar S-parameter measurements but is of fundamental importance to the entire microwave design and circuit community.
- Develop calibration substrates and algorithms for planar scattering parameter measurements up to at least 325 GHz. This was achieved by fully characterising calibration standards built in selected substrate materials through dimensional measurements, wideband substrate permittivity extraction and numerical simulation. Guidelines have been developed to suppress the excitation of unwanted parasitic modes.
- Develop suitable calibration standards and methods for measurements of RF nano-devices. These addressed issues such as the impedance mismatch problem for calibrated S-parameter measurements of nano-devices and also the challenge of probing at nanoscale dimensions.
- Engage with manufacturers of planar microwave circuits and components to facilitate the take up of the technology and measurement infrastructure developed by the project. This has been achieved by actively engaging such manufacturers in technical work packages and by developing best measurement practice guidelines, which serve the entire on-wafer measurement community.

4 Results

4.1 Objective 1: Establish traceability of planar scattering parameter measurements on reference calibration substrates

Traceability forms the basis for credible measurement results and their associated uncertainties. It is driven by today's global economy needs and usually achieved by an unbroken chain of comparisons, to stated references, typically in the form of standards by national metrology institutes (NMIs) or designated laboratories.

In contrast to coaxial and rectangular waveguide S-parameter measurements, traceability for on-wafer S-parameters has not been fully established prior to this project. This is because planar devices and calibration standards are fabricated on different substrate materials in a great variety of technologies, and instead of standardised connectors nowadays a number of microwave probes from several vendors can be used. Therefore, reliable uncertainties for on-wafer scattering parameters (S-parameters) can only be specified in a given environment for selected combinations of substrate materials, planar waveguides, and probes.

The aim was to provide the lowest possible uncertainties for S-parameter measurements of devices embedded on the same wafer, and to quantify the uncertainties. Candidates for reference calibrations, such as airline-like interconnects in membrane technology and substrates such as GaAs which allow for comparisons to electro-optic waveform metrology, have been evaluated. As a world-wide first, traceability was demonstrated not only for devices built in membrane technology, but also on a conventional thin-film substrate used in industrial applications (fused silica).

4.1.1 Traceability for calibration substrates built in membrane technology

The work initially focused on planar devices built in membrane technology, as the influence of the thin supporting dielectric material is significantly reduced in comparison to the influence of several-hundred- μm thick substrates which are conventionally used. In essence, membrane technology enabled us to employ airline-like coplanar waveguides (CPWs) as calculable calibration standards.

The employed high-resistivity silicon (HRSi) reference calibration substrate was fabricated in membrane technology and equipped with a multitude of different planar one-port and two-port test structures, designed as coplanar waveguide structures and reflective devices, serving as calibration standards and devices under test (DUT) as well. Figure 1.1 shows an interconnect structure serving as Thru calibration standard consisting of silicon-to-membrane transitions at both sides of a coplanar waveguide section supported by a thin membrane. The silicon-to-membrane transitions contain contact pads, which allow for ground-signal-ground microwave probing, and a short interconnect segment on silicon.

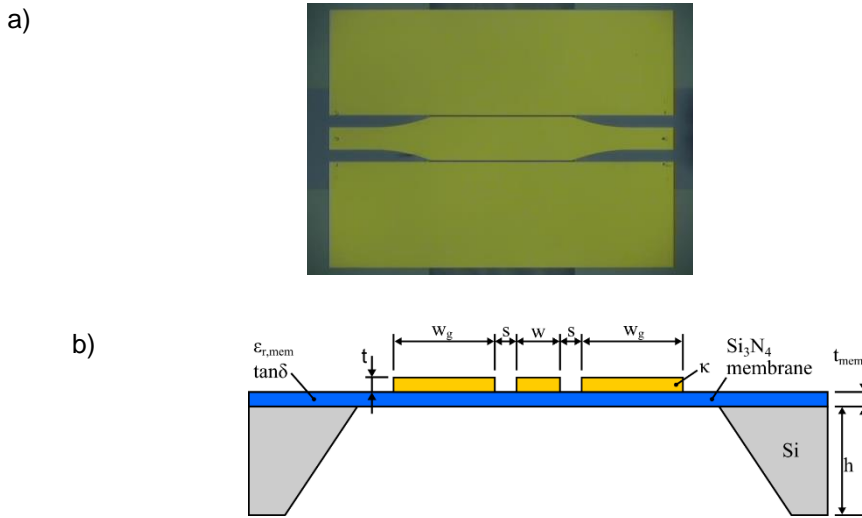


Figure. 1.1: Thru calibration standard built in membrane technology on a high-resistivity silicon substrate: a) Top view (photograph), b) Schematic of cross section (dimensions not scale).

Measurements were performed utilizing an Anritsu VectorStar vector network analyzer (VNA) with millimetre-wave extension modules for frequencies up to 125 GHz, connected to GGB ground-signal-ground microwave probes with 100 μm pitch. A comprehensive uncertainty budget has been established considering fabrication tolerances of the calibration standards as well as influences of the entire measurement setup.

The evaluation of S-parameter uncertainty depends on a number of factors such as instrumentation errors, cable and connector repeatability, standard uncertainties, the calibration algorithm chosen, and the DUT itself. This complicated task is greatly simplified with modern software tools such as the NIST Microwave Uncertainty Framework or METAS VNATools II. In our approach, we established a comprehensive uncertainty budget for the entire measurement process using the linear uncertainty propagation library Metas.Unclib which is based on the automatic differentiation techniques of.

For the calculation of corrected S-parameters from the measured raw data and the propagation of measurement as well as calibration standard uncertainties to the final results, the VNA measurement model described in EURAMET Calibration Guide No. 12 (CG-12) has been applied.

Figure 1.2 shows a block diagram of the general N-port measurement model (in our case N=2). The symbols M, R, W, V, E, D, C and S denote the raw data measured by the VNA, the noise and linearity influences, the switch terms, the drift of the switch terms, the calibration error terms, the drift of the calibration error terms, the cable stability and connector repeatability and DUT uncertainty influences, and the error corrected data (or calibration kit standard definitions), respectively.

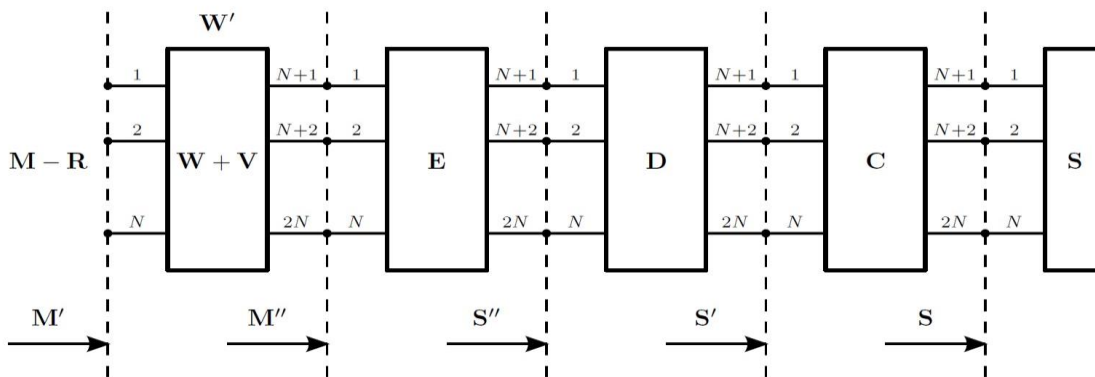


Figure 1.2: VNA measurement model (from EURAMET CG-12).

The error terms of the underlying 7-term error model were calculated with the multiline Thru-Reflect-Line (TRL) calibration algorithm introduced by R.B. Marks in 1991. Seven lines with membrane CPW lengths between 500 and 20190 μm were used, assuming a length uncertainty of 10 μm. Due to the lack of resistive elements

in the membrane technology used for the test wafer, the crosstalk correction of D.F. Williams et al., 2014, could not be applied. Instead, the DUT uncertainty approximation as described in the documentation of METAS VNATools II has been employed.

All relevant input quantities such as instrumentation influences, connection repeatability and calibration standard uncertainties were characterised with the best possible techniques. Characterisations of the VNA measurement setup were performed following the procedures outlined in EURAMET CG-12. Dimensional characterisation was carried out with a high-precision optical coordinate measuring machine and an atomic-force microscope (AFM). Typical values for the input quantities of the measurement model and their uncertainties are given in a recent ARFTG conference article, where traceability was demonstrated for several devices such as matched lines and offset reflects fabricated in membrane technology.

Figure 1.3 compares measured and model-based values of reflection and transmission S-parameters of a 500 μm -long matched line. Solid lines indicate nominal values, shaded areas indicate the expanded uncertainty intervals at a coverage probability of 95% ($k=2$). The S-parameters are normalized to 50 Ω . The expanded uncertainty intervals fully comprise the model values in the frequency range from 1 to 110 GHz.

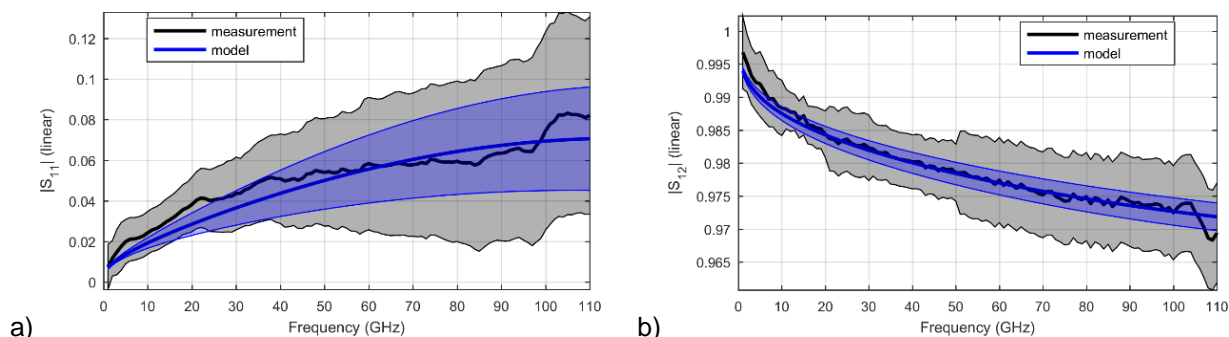


Figure 1.3: Comparison between measured (black) and modeled (blue) S-parameters of a 500 μm -long matched line: a) magnitude of reflection S-parameter, b) magnitude of transmission S-parameter.

4.1.2 Electro-optic waveform metrology

High-frequency devices are usually characterised in the frequency domain using electronic vector network analysers. Yet, the advent of femtosecond laser technology also enabled the characterisation of such devices in the time domain. Corresponding methods have already been employed for the characterisation of oscilloscopes or photodiodes. Although laser-based optoelectronic techniques have an incredibly large bandwidth and are assumed to provide traceability to the SI, corresponding verification does not exist.

Recently, a one-port laser-based optoelectronic VNA was demonstrated, where femtosecond laser pulses were used to measure voltage signals in the time-domain on a planar waveguide. The separation between forward and backward propagating signals, being the key task of VNAs, was realised by measuring voltage signals at different positions on the planar waveguide. With this improvement laser-based techniques could now be used to perform vector network analysis.

In a first comparison a device under test (DUT) was characterised using both, laser-based and conventional VNAs. To this end, specialised structures addressing the needs of both measurement techniques (laser-based electro-optic sampling (EOS) and conventional) were implemented on a low-temperature-grown gallium arsenide (LT-GaAs) substrate.

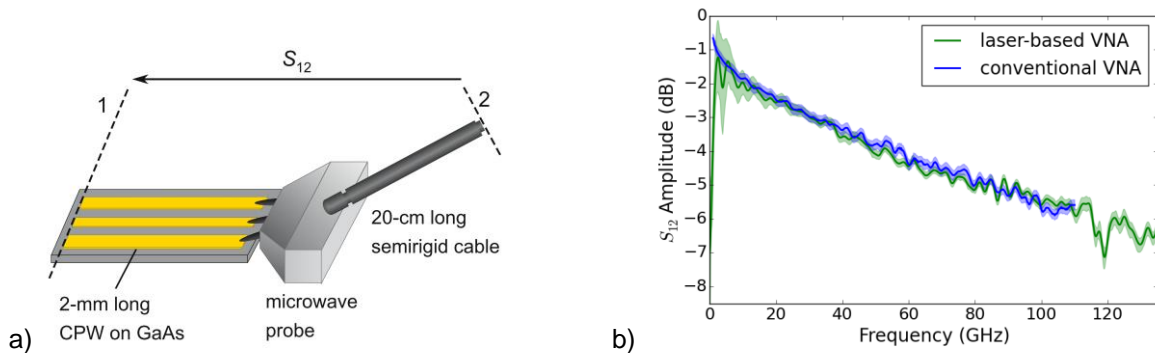


Figure 1.4: Comparison between time- and frequency-domain high-frequency device characterizations: a) Device under test and definition of scattering parameters, b) Amplitude of S_{12} of the DUT obtained from the time- and frequency-domain techniques (thick lines). The 95% confidence intervals are marked by the light semi-transparent colors.

The DUT consisted of several different elements and is pictured in Figure 1.4a. A 20-cm long semi-rigid cable is connected to a coaxial-coplanar microwave probe both having 1.0-mm coaxial connectors. The microwave probe is attached to a 2-mm long coplanar waveguide. While the end of the CPW constitutes port 1 with a characteristic impedance being complex at low frequencies, the end of the coaxial semi-rigid cable constitutes port 2 with a characteristic impedance taken as 50Ω . The comparison focussed on the S_{12} scattering parameter, with the characteristic port impedances as noted above, i.e., no impedance transformation was performed.

For the frequency-domain measurement of S_{12} the DUT of Figure 1.4a was split up in two parts: the planar-coaxial part consisting of the 2-mm CPW length and the microwave probe, and the 20-cm semi-rigid cable part with coaxial 1.0-mm ports. For characterising the semirigid cable a two-port 1.0-mm calibration was first performed as recommended by the manufacturer of the broadband VNA system (Anritsu VectorStar). This calibration consisted of a low-band and high-band part employing different calibration standards suitable for the respective band, which were merged afterwards to provide the bandwidth from 1 to 110 GHz used in this experiment. For characterising the planar-coaxial part, a two-port second-tier procedure was used.

The amplitude of the DUT's S_{12} parameter obtained from both the time- and frequency domain methods are shown in Figure 1.4b. With the conventional VNA we obtained data up to 110 GHz limited by the calibration-kit definitions provided by the manufacturer. The effective bandwidth of the time-domain VNA was mainly limited by the width of the ultrashort voltage pulses. This first comparison between both measurement methods demonstrated good agreement in the frequency range from 10 GHz to 110 GHz, although the 95% confidence intervals did not overlap at every frequency point.

For comparison measurements on purely planar devices, however, unexpected artefacts showed up in the frequency domain results of the EOS measurements at frequencies below 110 GHz. Despite extensive investigations, the origin of this artefacts could not be found. This rendered the EOS approach as currently unusable for providing traceability.

4.1.3 Traceability for coplanar waveguide calibrations on fused silica substrates

In the project, a major effort has been undertaken to better understand the limitations in the accuracy of planar S-parameter measurements. To this end, parasitic modes as well as effects occurring at higher frequencies such as radiation, dispersion and surface roughness have been investigated together with the impact of the probe itself and its neighbourhood. All the investigations confirmed that the measurement result depends on the environment as well as on the specific combination of substrate material, planar waveguide type, and probes. Only for such fully specified combinations, and only when single-mode propagation is ensured, reliable uncertainties for on-wafer S-parameters can be stated.

To extend the traceability path used for membrane technology devices to conventional devices built on typical microwave substrates such as e.g. fused silica, the dielectric influence of the substrate material had to be taken fully into account. This necessitated the wideband extraction of the complex permittivity in the entire frequency range from 1 to 110 GHz. To this end, three different sources of information were considered (see Figure 1.5). As the uncertainties of the wideband dielectric measurement methods have not yet been fully established, conservative estimates were used for the relative permittivity ϵ_r and the loss tangent $\tan \delta$ based

on the results of Figure 1.5. For both quantities a uniform probability density function was assumed. The resulting values used for the entire frequency range under consideration were $\epsilon_r = 3.78 \pm 0.15$ and $\tan \delta = (8 \pm 7)10^{-4}$.

To achieve highest precision in the dimensional characterisation of the calibration standards, atomic-force microscopy was used.

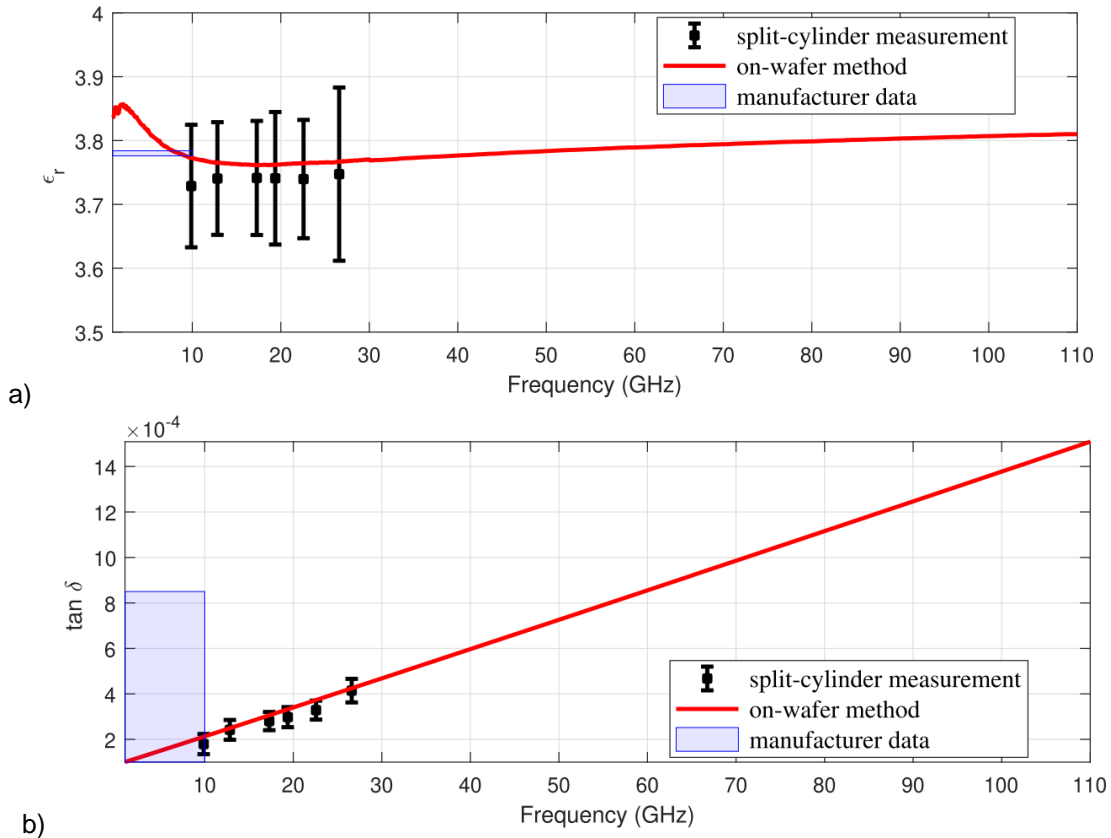


Figure 1.5: Dielectric material characterization for the fused silica substrate: a) relative permittivity, b) loss tangent.

In Figure 1.6 results for three typical devices are shown, covering a large portion of the impedance range measurable by a VNA: a nominally 15 dB matched attenuator (termed ‘attenuator’), a 7000 μm -long mismatched line (termed ‘mismatch’), and a 2-port open (high-reflect device, termed ‘open’). Figure 5 shows expanded uncertainty intervals at a coverage probability of 95% ($k=2$) of the reflection magnitude for all three devices considered. All S-parameters were normalised to the system reference impedance of 50 Ω . Even though relatively large uncertainties in the dielectric properties of the substrate were assumed, the resulting uncertainties are only slightly larger in comparison to the membrane technology case. This can be partially explained by the better accuracy in the dimensional AFM measurements on the fused silica substrate.

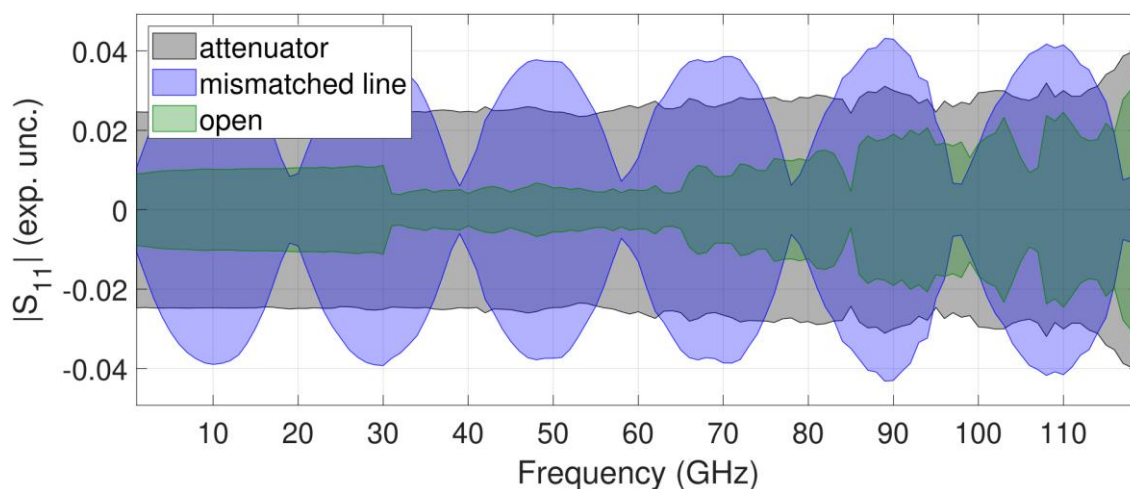


Figure 1.6: Expanded uncertainty intervals at a coverage probability of 95% ($k=2$) for the magnitude of S_{11} of three devices on fused silica.

PTB is currently preparing Calibration and Measurement Capabilities (CMC) entries for traceable 2-port S-parameter measurements of fused silica and membrane technology devices. The methodology developed can be extended to other substrate materials used in industry such as e.g. alumina or GaAs. PTB will be the first NMI worldwide able to offer calibration services for planar S-parameter measurements to industry.

4.2 Objective 2: Transfer uncertainties to calibration standards in conventional technology to be used in industry

Methods to transfer uncertainties from reference calibration substrates to working calibration substrates are essential for industrial applications. The aim is to preserve the low uncertainties in S-parameter measurements achieved on custom-made reference calibration substrates even when using low-cost working calibration substrates, such as e.g. impedance standard substrates (ISSs), which can be purchased from several on-wafer vendors. Two approaches have been initially under investigation which can potentially transfer uncertainties from a reference calibration substrate to a working calibration substrate: permittivity compensation and residual error estimation. Work on both approaches on a range of devices, showing that the range of improvements is quite limited, is presented in the following.

Additionally, a third option has been explored which allows for transferring uncertainties to industrial applications where commercial ISSs and simple calibration algorithms have to be used. Here, one has to first characterise the standards in a manner which is adequate for the target application. This requires building custom calibration standards on the target DUT wafer, which serve for characterising the ISS calibration standards appropriately. The feasibility of this approach was demonstrated for the case of alumina substrates. The results of a reference calibration using custom standards were in essence duplicated with the aid of characterised ISS standards and a much simpler, industrial calibration. The uncertainties of the industrial calibration only slightly increased compared to the uncertainties of the reference calibration.

4.2.1 Substrate permittivity compensation

In a 1994 ARFTG conference paper, D.F. Williams et al. developed a simple capacitance model to account for the effect of a change in substrate permittivity on coplanar waveguide TRL calibrations performed on different substrate materials. For all calibrations, the reference plane was moved to the probe tip and the reference impedance was set to 50Ω . Whereas in the 1994 ARFTG conference paper all cross-sectional dimensions of the CPWs on the different substrates were assumed identical, a later investigation demonstrated that also the measurement error caused by differences in the conductor geometry can be accounted for. As the measurements were limited to the 40 GHz frequency range, we investigated the performance of this compensation technique using custom-made fused silica and alumina substrates up to 110 GHz.

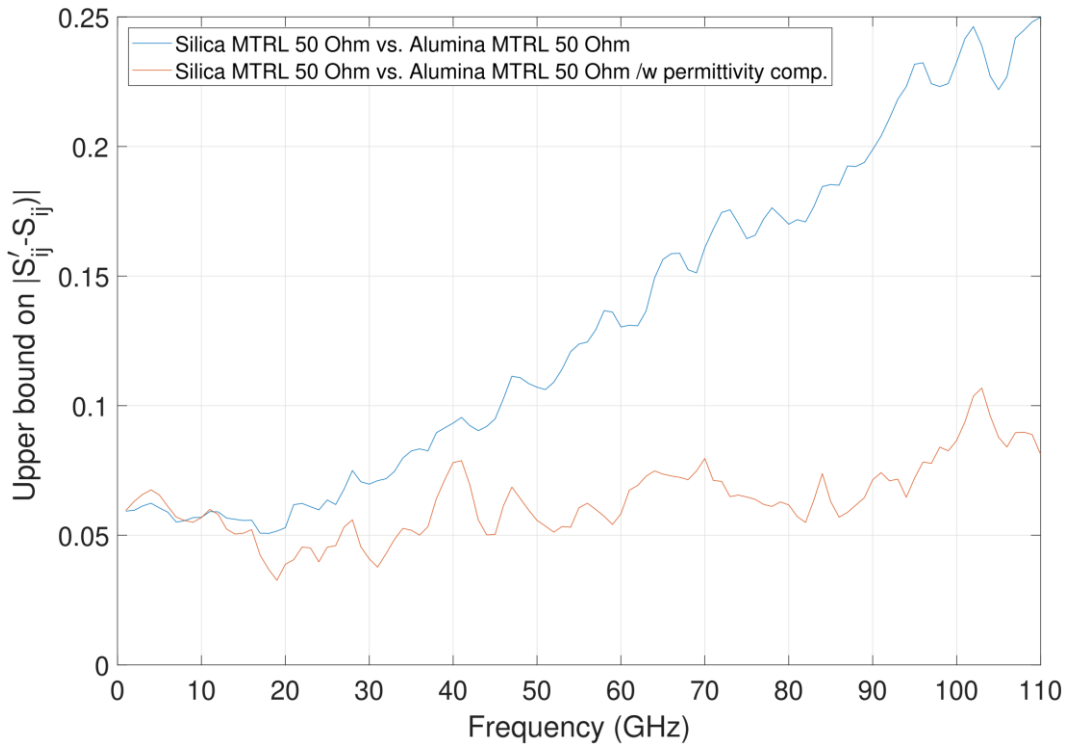


Figure 2.1: Worst-case error bounds calculated by calibration comparison method.

Figure 2.1 shows the worst-case error bounds calculated for multilayer TRL calibrations using the calibration comparison method on the two different wafers before (blue) and after (red) applying the substrate permittivity compensation technique described above. The red curve shows a significant reduction of the error bound after applying the permittivity compensation. As the calibration comparison technique tends to overestimate the actual errors in the measurements, we decided to investigate the actual deviations from the reference measurement result on alumina before and after applying the substrate permittivity compensation.

To this end, we investigated measurements of different devices fabricated on the alumina wafer in the frequency range from 1 to 110 GHz (see Figures 2.2-2.3). The multilayer TRL calibration on the alumina wafer gives the most accurate result (black curves), while the multilayer TRL calibration on the fused silica wafer (brown curves) will introduce a systematic error due to the differences in substrate permittivity and conductor geometries. The red curves show the result for the multilayer TRL calibration on the fused silica wafer after applying the substrate permittivity compensation technique. In the case of one-port devices only the results for reflection are shown.

Figure 2.2 shows the results for a one-port device, an offset open. The permittivity compensation only improves the phase of S_{11} . The compensation does not work for the magnitude of S_{11} , and again, for frequencies above 60 GHz, the systematic errors in the magnitude of S_{11} start to increase with frequency.

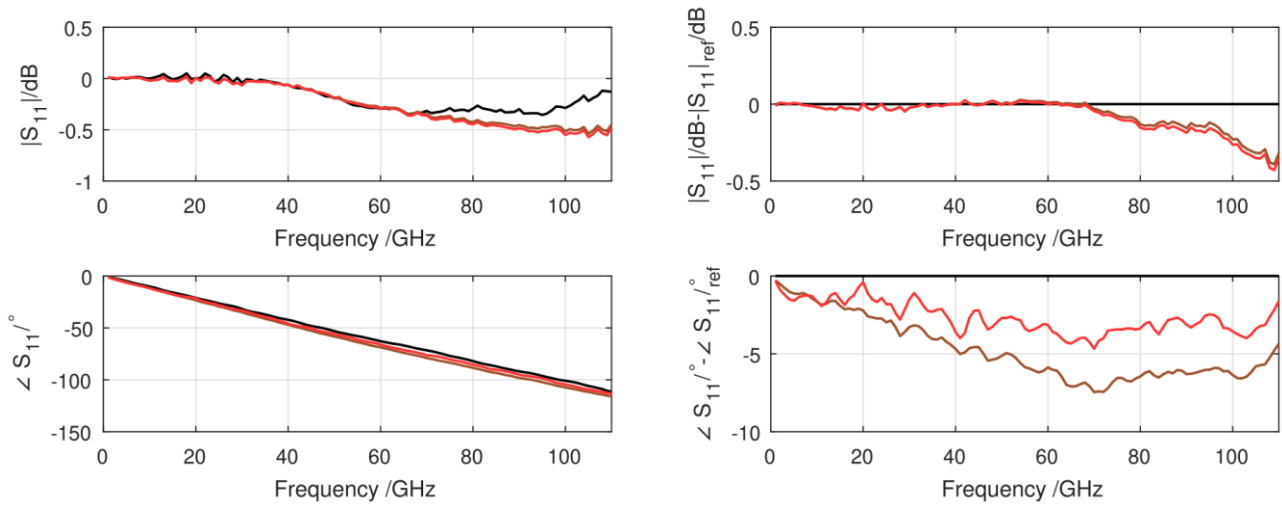


Figure 2.2: Reflection measurement of open device on alumina: left) Magnitude and phase of S_{11} , right) Measurement normalized to reference mTRL result on alumina (colors: black-reference mTRL on alumina, brown-mTRL on fused silica, red-mTRL on fused silica after permittivity compensation)

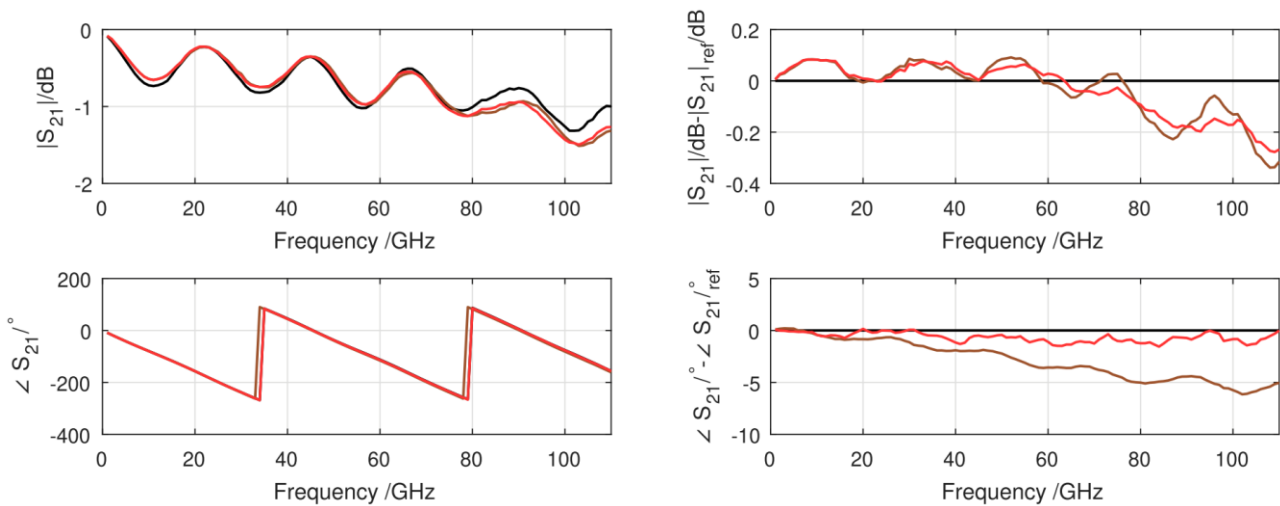


Figure 2.3: Transmission measurement of mismatched line on alumina: left) Magnitude and phase of S_{21} , right) Measurement normalized to reference mTRL result on alumina (colors: black-reference mTRL on alumina, brown-mTRL on fused silica, red-mTRL on fused silica after permittivity compensation)

Similar results were found also for 2-port devices. As an example, Figure. 2.3 shows the transmission measurement of a mismatched line on alumina. Again, the corrective effect of the permittivity compensation is more notable in the phase, and for frequencies above 60 GHz, the errors in the magnitude of S_{21} cannot be compensated.

In summary, one can state the permittivity compensation technique mostly improves on the phase error introduced by the on-wafer calibration on fused silica. The effect is generally more notable in S_{21} compared to S_{11} . With regard to the magnitude error, which increases for frequencies above 60 GHz, almost no improvement can be found.

4.2.2 Residual error correction

A more general approach for compensating systematic errors introduced by the VNA calibration is the determination of residual errors and the application of a second-order error correction afterwards. In a conference paper by A. Savin et al. presented at the 84th ARFTG conference, a method for determining complex residual errors of two-port VNA calibrations was described which makes use of a time-domain approach. The residual errors are extracted from a distance-frequency system model using a special estimation algorithm based on the quasi-optimal unscented Kalman filter. Since the method requires only three

measurement conditions, it is particularly suited for on-wafer applications, as these conditions can be obtained from using only one verification line. In a more recent conference paper by A. Savin presented at the 47th European Microwave Conference 2017, the same measurement conditions are exploited, but since the residual error terms are now estimated by applying a least-mean-squares method the calculation time is significantly reduced.

Here, we determined the residual errors of calibrated two-port on-wafer measurements up to 110 GHz with the more recent method, utilizing the commercial calibration substrate GGB CS5 and GGB100 microwave probes. As verification line, line 10 with a length of 6600 μm was used. As DUTs lines of different lengths in the range 550 to 1500 μm were used. By analysing the error-corrected measurements of the DUTs, we compared the accuracy of SOLT calibrations with characterised standards to SOLT calibrations with manufacturer definitions and to second-order-corrected SOLT calibrations with manufacturer definitions. In the following figures, the error-corrected reflection and transmission measurement are shown on the left-hand side, while the differences with regard to the reference calibration (SOLT with characterised standards) are shown on the right-hand side.

Figure 2.4 shows exemplarily the results for the line length of 1500 μm . One obvious disadvantage of the second-order error correction becomes apparent for frequencies below 10 GHz: additional errors are introduced leading to unphysical behaviour in both reflection and transmission. For higher frequencies, however, the second-order correction is mostly working as expected. In the measured reflections, the second-order error correction is beneficial, as can be seen from the red S_{11} curves approaching the black S_{11} curves in a range from approximately 20 to 110 GHz. In the measured transmission, there is almost no improvement for the magnitude of S_{21} .

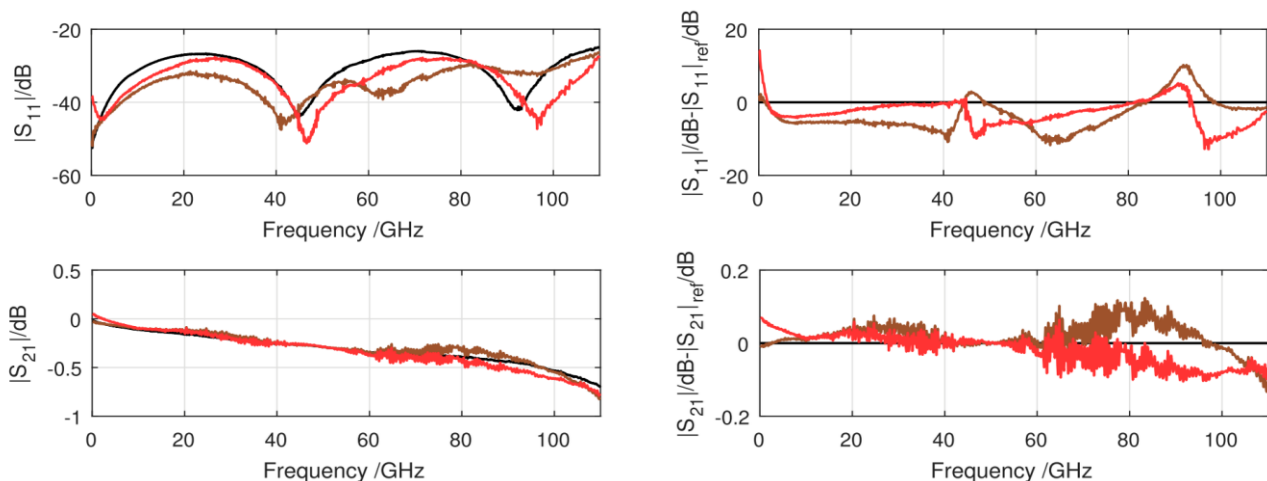


Figure 2.4: Reflection and transmission measurement of 1500 μm long line on GGB CS-5 substrate: left) Magnitudes of S_{11} and S_{21} , right) Measurements normalized to reference Short-Open-Load-Thru (SOLT) result with characterized standards (colors: black-reference SOLT with characterized standards, brown-SOLT with manufacturer definitions, red- SOLT with manufacturer definitions after residual error correction)

In a recent article at the CEMi'18 International Workshop on Computing, Electromagnetics, and Machine Intelligence, 2018, we demonstrated that independent of the calibration standard definition and the calibration method used, consistent results are obtained after applying the residual error correction introduced by Savin. In summary one can state that the second-order error correction of Savin shows some promise but is currently limited by the accuracy with which the residual errors can be determined. At the edges of the frequency range (ca. 5% of the frequency band), the error of the filtering algorithm increases. This applies to measurements of both transmission and reflection coefficients. In principle, the effect can be reduced by applying a verification line with a longer length.

The current study was limited by the number of DUTs and the verification line available on the commercial calibration substrate. Future investigations should try to extend the study to better understand and overcome the current limitations of the method of Savin.

4.2.3 Transfer of uncertainties with the aid of ISS

In a recent article presented at the 91st ARFTG conference, we demonstrated that properly characterised standards can be used to account for differences between the commercial ISS and the target DUT measurement situation. The results of a reference mTRL calibration using custom standards were in essence duplicated with the aid of characterized ISS standards and a much simpler calibration, in this case SOLT. This constitutes a big improvement over any of the approaches discussed in the two previous subsections, where a systematic error with regard to the reference result remained.

Therefore, in order to transfer uncertainties to industrial applications where commercial ISS substrates and simple calibration algorithms have to be used, one has to first characterise the standards in a manner which is adequate for the target application. This requires building custom calibration standards on the target DUT wafer, which serve for characterising the ISS calibration standards appropriately. In the following, we demonstrate this approach with the custom-made alumina wafer as the target DUT wafer and the GGB CS5 calibration substrate as commercially available ISS substrate.

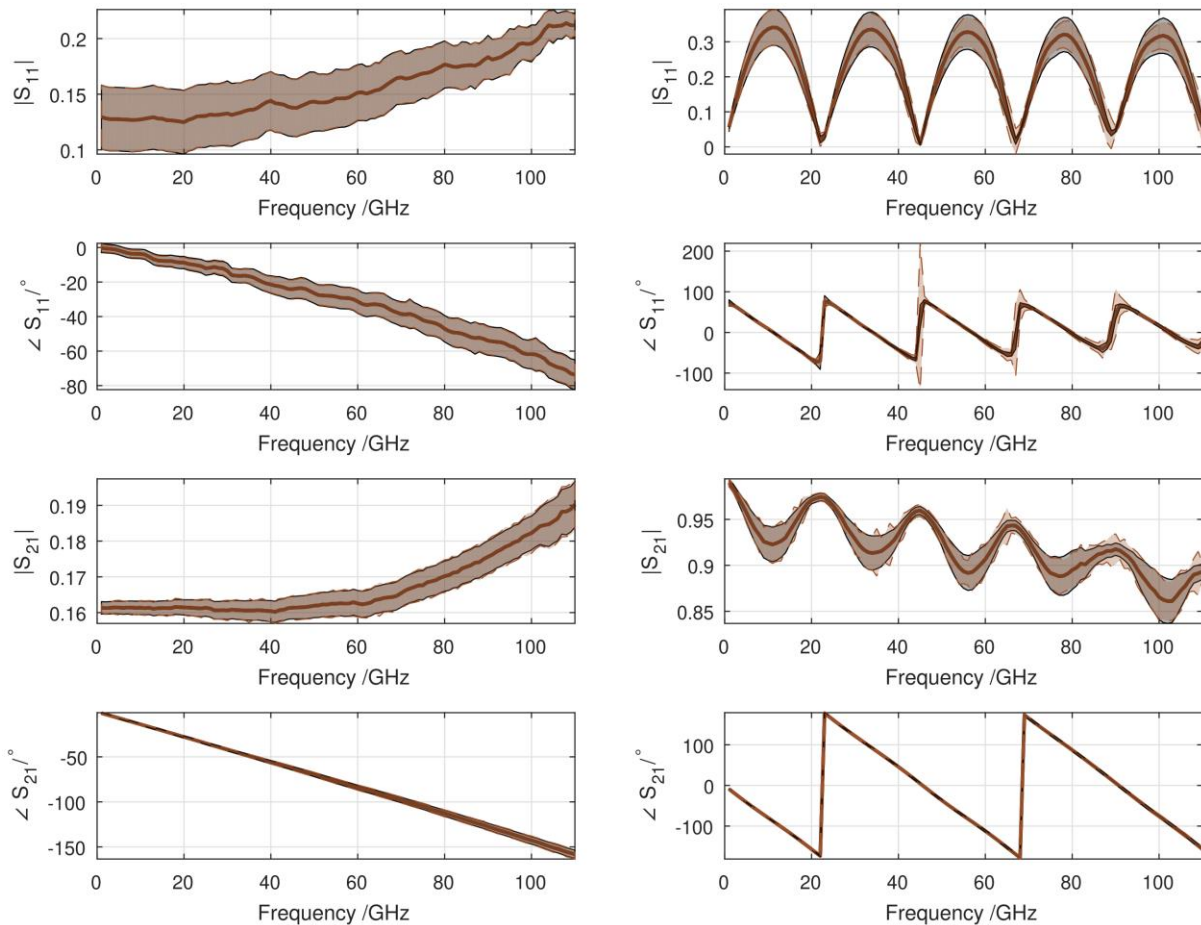


Figure 2.4: Reflection and transmission measurement on alumina substrate: left) Attenuator, right) Mismatched line (colors: black-reference mTRL calibration on alumina, brown - SOLT calibration with characterized CS5 standards)

The traceability path developed by PTB for on-wafer S-parameter measurements is based on the multiline TRL calibration algorithm (see Section 4.1). The methodology can also be applied to other substrates, as long as the wideband material properties are known and single-mode propagation can be assumed. For the custom-made alumina wafer used in our studies, the latter condition is strictly fulfilled only for frequencies below ca. 70 GHz. For higher frequencies, the effects of dispersion and interaction with higher-order and other parasitic modes are currently not fully captured in the uncertainty budget. Nonetheless we used this preliminary uncertainty budget and treated the alumina wafer as reference calibration wafer for characterising the standards on the CS5 substrate by GGB industries.

Figure 2.4 compares the measurement results for an attenuator DUT and a mismatched line DUT fabricated on the alumina wafer. The black curves show the reflection and transmission when using the reference mTRL

calibration on the alumina substrate, the brown curves show the corresponding results for the SOLT calibration with the characterised CS5 standards. The shaded areas indicate the expanded uncertainty intervals. It can be clearly seen that the nominal values coincide for both calibrations, proving the consistency of the approach. The only differences appear in the expanded uncertainties, which are usually slightly increased for the calibration with the characterised standards.

Exemplary uncertainty budget values for the DUTs corrected via the SOLT calibration with characterised CS5 standards are given in the Table 2.1. These tables show the uncertainty budget composition for the magnitude of S_{11} of the DUTs at a frequency of 65 GHz. The calibration standard uncertainties are designated with PTB_ML in the beginning, pointing to the fact that the characterisation was performed with the PTB multiline calibration. The tables clearly show that the budgets are mostly dominated by the calibration standard uncertainties.

Description	Unc Component	Unc Percentage	Description	Unc Component	Unc Percentage		
Cable Stability	0.001450124	0.000	Cable Stability	0.058828227	0.083		
Calibration Standards:	0.670126203	99.592	Calibration Standards:	2.039187357	99.639		
⇒ PTB_ML_CS5_open_51 S11	0.058003624	0.746	⇒ PTB_ML_CS5_open_51 S11	0.023740527	0.014		
⇒ PTB_ML_CS5_open_51 S22	0.001496587	0.000	⇒ PTB_ML_CS5_open_51 S22	0.070263207	0.118		
⇒ PTB_ML_CS5_res_71_50 S11	0.666248662	98.443	⇒ PTB_ML_CS5_res_71_50 S11	1.883437737	85.000		
⇒ PTB_ML_CS5_res_71_50 S22	0.002807877	0.002	⇒ PTB_ML_CS5_res_71_50 S22	0.125927050	0.380		
⇒ PTB_ML_CS5_short_61 S11	0.038046580	0.321	⇒ PTB_ML_CS5_short_61 S11	0.049882933	0.060		
⇒ PTB_ML_CS5_short_61 S22	0.001042205	0.000	⇒ PTB_ML_CS5_short_61 S22	0.058699120	0.083		
⇒ PTB_ML_CS5_thr_81 S11	0.018936710	0.080	⇒ PTB_ML_CS5_thr_81 S11	0.763456399	13.966		
⇒ PTB_ML_CS5_thr_81 S12	0.000143966	0.000	⇒ PTB_ML_CS5_thr_81 S12	0.006792718	0.001		
⇒ PTB_ML_CS5_thr_81 S21	0.000143964	0.000	⇒ PTB_ML_CS5_thr_81 S21	0.006792700	0.001		
⇒ PTB_ML_CS5_thr_81 S22	0.000184802	0.000	⇒ PTB_ML_CS5_thr_81 S22	0.026407654	0.017		
Connector Repeatability	0.039950930	0.354	Connector Repeatability	0.106121881	0.270		
DUT Uncertainty	0.000055924	0.000	DUT Uncertainty	0.001340632	0.000		
VNA Drift (Ideal VNA correlated)	0.015253581	0.052	VNA Drift (Ideal VNA correlated)	0.014373846	0.005		
VNA Linearity	0.000000000	0.000	VNA Linearity	0.000000000	0.000		
VNA Noise	0.002606109	0.002	VNA Noise	0.011795602	0.003		
a)	Value: -16.245	Std Unc: 0.671	U95: 1.342	b)	Value: -19.804	Std Unc: 2.043	U95: 4.086

Table 2.1: Uncertainty budget for magnitude of S_{11} for attenuator (a) and mismatched line (b) at 65 GHz (in dB).

4.3 Objective 3: Improve planar transmission lines models accounting for surface roughness and radiation losses

Accurate transmission-line models are indispensable for the design of calibration standards and for the corresponding algorithms. Improving planar transmission line models taking into account surface roughness as well as radiation losses and dispersion effects help to develop reliable uncertainty budgets for planar S-parameter measurements and will be of fundamental importance to the entire microwave circuit design community. Presently, these models do not, or only to a limited extent, include the high-frequency phenomena related to conductor roughness and radiation. In the framework of the PlanarCal project a thorough study of the surface roughness and radiation effects in the higher GHz frequency range has been performed and the existing transmission line model has been adapted including these effects. The phenomena of surface roughness on the one hand and dispersion and radiation on the other hand can be studied independently from each other.

4.3.1 Dispersion and Radiation

While at lower frequencies dispersion and radiation effects are negligible, they become an important issue with increasing frequencies when the transversal dimensions are no longer small compared to wavelength and the quasi-TEM assumptions do no longer apply. For this reason, the coplanar waveguide (CPW) case was studied in detail, using 3D full-wave electro-magnetic (EM) simulations as a reference to validate the existing transmission line model.

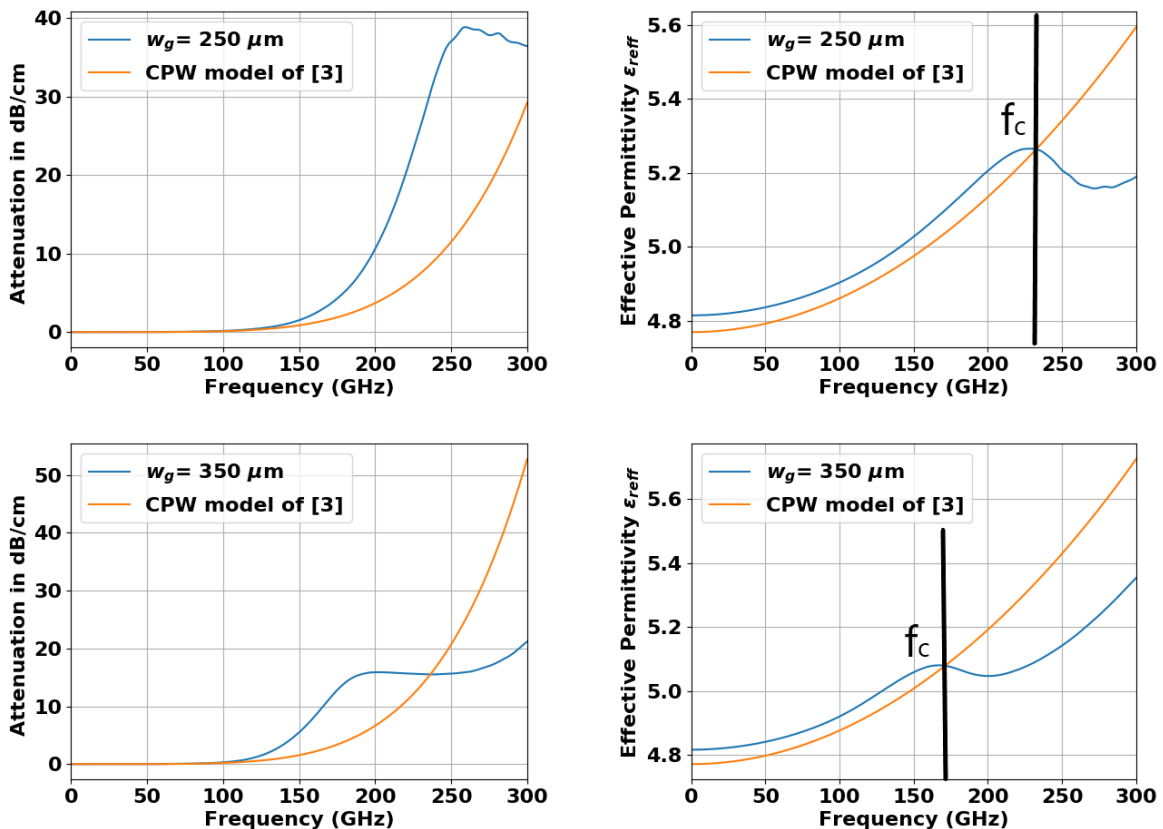


Figure 3.1: Propagation constants for a CPW with $w = 50 \mu\text{m}$, $s = 25 \mu\text{m}$ with $w_g = 250 \mu\text{m}$ ground width (top) and $w_g = 350 \mu\text{m}$ ground width (bottom), 3D simulation data (blue) and results of the CPW model of Schnieder et al., 2003 (orange). The upper frequency limit f_c is marked in the graphs (see Figure 3.1 right).

The EM simulations were performed using the software Microwave Studio by CST which is based on the Finite Integration Technique (FIT). In order to model a realistic measurement scenario, CPW structures on infinitely thick substrates were considered, which is comparable to the measurement set-up on a ceramic chuck. The frequency range up to 300 GHz was covered. Perturbations by artificial modes caused by the simulation boundaries are excluded by applying a 3D approach: The structures are excited through internal ports and the

entire simulation domain is enclosed by PML absorbing boundaries (PML: perfect matched layers). For the excitation, a simplified bridge model has been used. The model has been verified for CPW structures in various scientific publications and thus represents a reliable reference.

In order to exactly reproduce measured results, the same procedure was followed: The simulations were performed for the full set of calibration elements, as in the measurement case, and then the resulting data was processed by a calibration algorithm, the multiline Thru Reflect Line (mTRL) calibration algorithm, which yields the propagation constants. This data is then compared to the results of the existing transmission line model, varying the parameters within a reasonable range.

4.3.1.1 Summary of the Results

Figure 3.1 shows examples for the results, allowing to assess the accuracy of the transmission line model. In this regard, one has to note that practical application of a transmission line model is limited to a certain frequency range, the upper limit of which is determined by the frequency f_c where interaction with the first higher-order mode occurs (see Figure 3.1 right). An empirical formula for this frequency was validated and implemented in the model. The approximation for dispersion in the conventional model was checked and a slight adaption of fitting parameters introduced based on our simulations. Validation shows excellent accuracy throughout the full parameter range. For radiation, deviations are more pronounced but considered to be acceptable for practical use within the reasonable frequency range.

4.3.2 Surface Roughness

The penetration of electromagnetic fields in conductive surfaces may be calculated analytically for an infinitely extended plane with an ideally smooth surface, which yields the well-known exponential decay of the field amplitudes and the so-called skin-depth δ_s :

$$\delta_s = \frac{1}{\sqrt{\pi\mu_0\sigma_{DC}f}} \quad (3.1)$$

where μ_0 denotes the vacuum permeability and σ_{DC} represents the bulk conductivity of the conductor. However, when δ_s reduces into the order of surface roughness, fundamental assumptions for the analytical derivation of the skin effect are no longer satisfied. As a consequence, significant deviations between calculated and measured losses are observed in various applications where smooth skin effect is considered within the calculation-models. Increases of losses by about 60% are often referenced in literature and even factors of more than 2 are reported. Furthermore, also the phase velocity is affected by rough surfaces producing additional deviations between models and measurements.

4.3.2.1 Interaction of EM Fields with Rough Surfaces

The interaction of electromagnetic fields with rough conductor surfaces can be predicted by the Gradient Model described by G. Gold and K. Helmreich in an IEEE Transactions on Microwave Theory and Techniques journal paper Oct. 2017. By assuming the transition of conductivity σ from the dielectric into the conductor to follow a certain function $\sigma(x)$ along the depth x (referred to as conductivity profile), starting from zero conductivity in the dielectric and reaching σ_{DC} inside the conductor, Maxwell's equations may be setup to represent that case. Although they deliver terms that are not solvable analytically in general, by applying a finite difference method this one-dimensional problem can be solved efficiently for arbitrary transition functions $\sigma(x)$. In most practical cases, the deviation of the actual surface from its mean value follows a normal distribution and, thus, the conductivity profile results in a cumulative density function CDF.

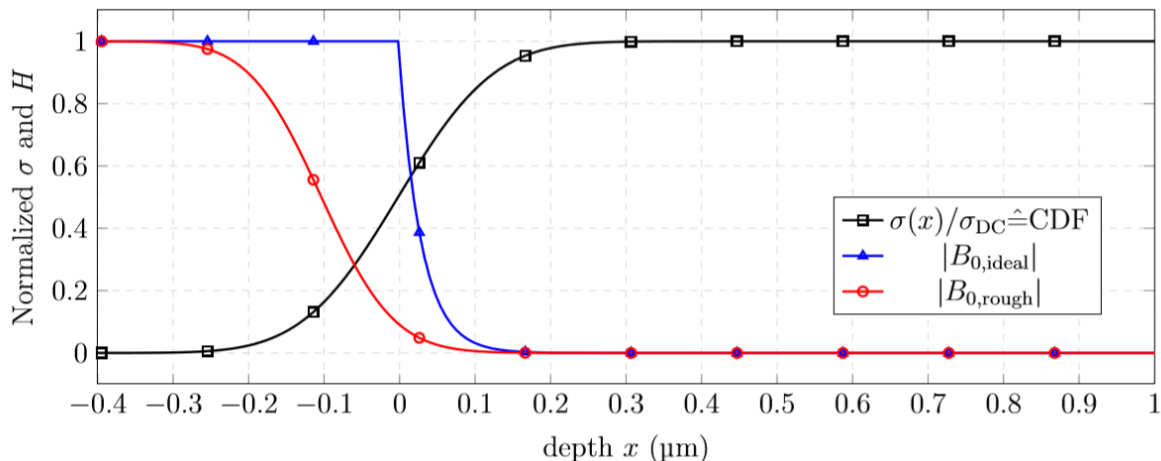


Figure 3.2. Conductivity profile and skin effect on smooth and rough surface at 50 GHz with $R_q = 1 \mu\text{m}$

The penetrating magnetic field as calculated by the Gradient Model is shown in Figure 3.2 and compared to the response calculated assuming the plane skin effect. As a consequence of the differences between smooth and rough responses of the magnetic field on the one hand and the non-constant conductivity profile on the other, magnetic field energy inside conductive media and conductor loss power density are no longer identically distributed over the penetration depth. Thus, the well-known relation for constant per unit length-parameters $L_i' = R'/\omega$ does no longer hold and the increase of inner inductance and conductor loss must be calculated separately in order to accurately take into account the impact of surface roughness on the propagating electromagnetic waves.

4.3.2.2 Modelling Rough Conductor Surfaces of Coplanar Waveguide (CPW)

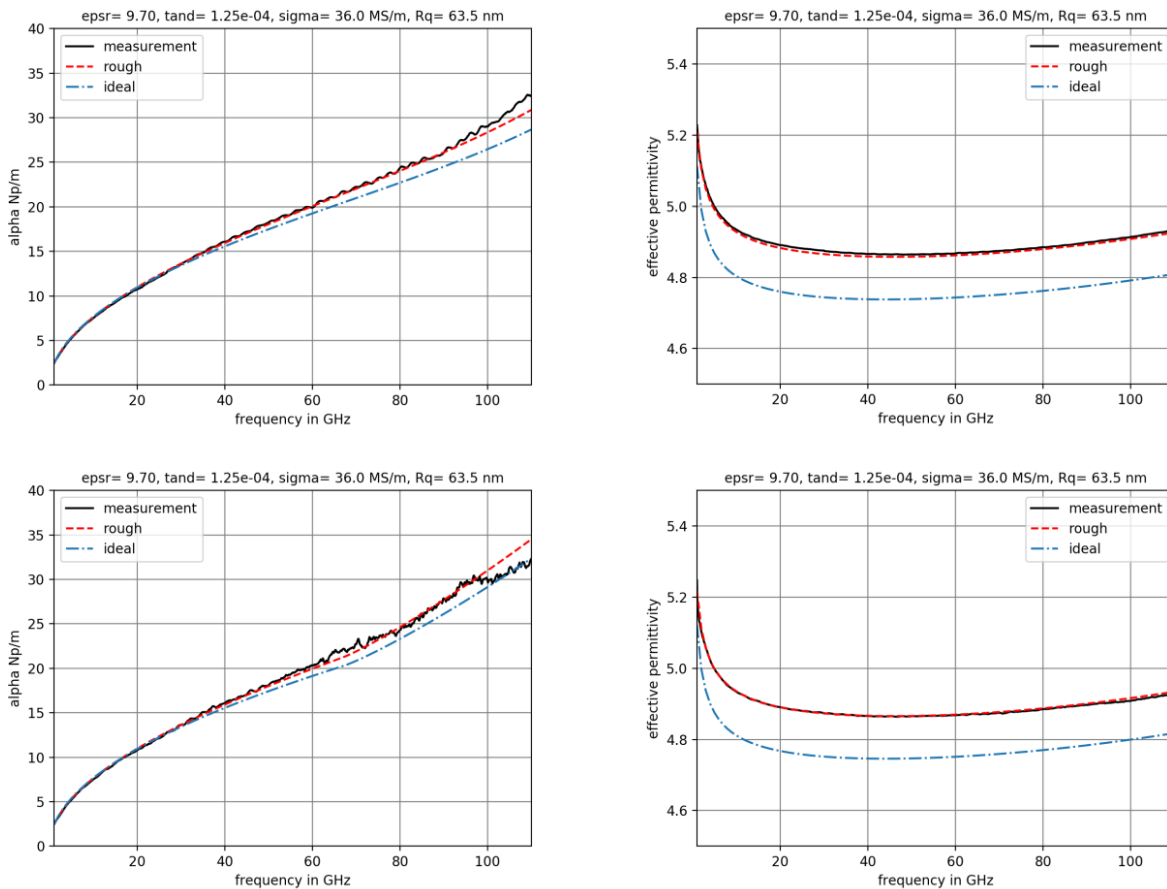
In order to make use of the existing CPW model from Schnieder et al. 2003, effective frequency dependent conductivity $\sigma_{\text{eff}}(f)$ and relative permeability $\mu_{r,\text{eff}}(f)$ are derived from the magnetic field response calculated by the Gradient Model. These virtual material properties that do not exist in reality can furthermore be applied to the conductor loss and inner inductance terms of the CPW respectively:

$$R' = \frac{\sqrt{\pi\mu_0 f}}{\sqrt{\sigma_{\text{eff}} \zeta}} \tag{3.2}$$

$$L_i' = \frac{\sqrt{\pi\mu_{r,\text{eff}} f}}{\sqrt{\sigma_{\text{DC}} \zeta \omega}} \tag{3.3}$$

where ζ represents a geometrical length that is related to the field distribution of among the circumference of the conductor and ground cross sections.

4.3.2.3 Validation of CPW model by Comparison with Measurements



4.4 Objective 4: Develop calibration substrates and algorithms for planar scattering

parameter measurements up to at least 325 GHz

One of the technical objectives of this project is to develop calibration substrates and algorithms for planar scattering parameter measurements up to at least 325 GHz. This is in response to the demand from industry. To achieve this objective, calibration standards have been fully characterised using dimensional measurements, extraction of permittivity over a wideband, and numerical simulations. Eight guidelines, concerning suppression of unwanted parasitic modes, have been developed. An example Thru-Reflect-Line (TRL) calibration kit has been designed following these procedures and tested over the frequency range of 75-325 GHz.

The guidelines are summarised below.

Multi-mode propagation

The high dielectric constant employed in commercially available substrates, together with the large gaps in the CPW design, leads to various unwanted modes being present in the lines used for probe level calibration in the frequency range above 110 GHz. Figure 4.1 shows the different propagating modes supported by a CPW. The critical frequency f_c , above which energy leaks from the nominal CPW mode to the un-wanted radiation mode, depends on various parameters: substrate permittivity, height and boundary conditions. The critical frequency can be calculated using equations, given in the IEEE Transactions on Microwave Theory and Techniques paper by Schnieder et al. (2003), which consider two cases: metal chuck and dielectric chuck. According to these equations, the higher the substrate permittivity, the lower the critical frequency will be. In the case of metal chuck, the usage of thin substrates helps shift the critical frequency to higher frequencies.

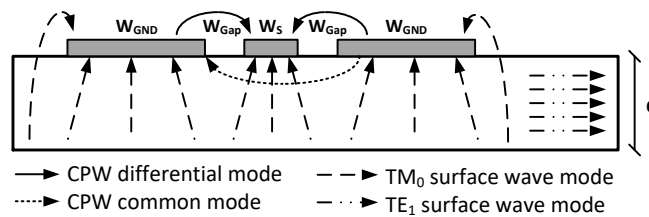


Figure 4.1: Cross section of a CPW with finite ground planes, and sketches of the E-field distributions of the first propagating modes supported.

Guideline #1: Compute the critical frequency (f_c) of the calibration substrate employed in the given configuration (i.e., metallic or dielectric chuck) and select those in which f_c is outside the calibration frequency or only occurs in the upper calibration range, to avoid excessive coupling of power to unwanted modes.

Boundary conditions (bounded-unbounded)

The effect of (i.e., error arising from) the presence of unwanted modes can be, to a first approximation, quantified by means of electro-magnetic (EM) simulations. The boundary conditions in a real environment will present effect comprised between the metal chuck condition (i.e., full reflection at the back side, providing a condition Figure 4.2 a) and the matched open boundary condition (i.e., infinite medium at the back side, providing a best case condition Figure 4.2 b). The difference of the worst case bound metric for these two cases can be used to provide a qualitative indication of the accuracy that the calibration on the given substrate can achieve.

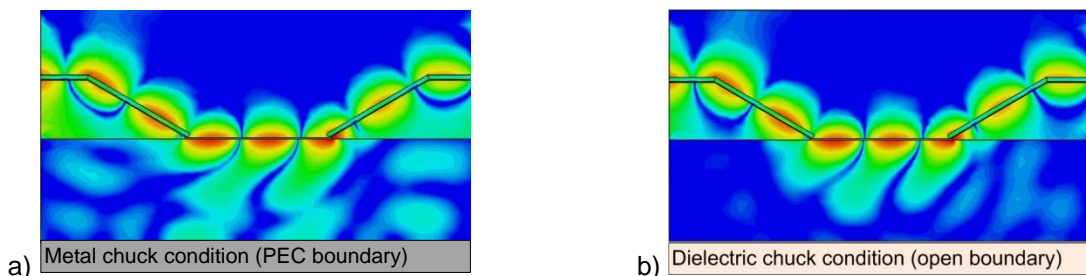


Figure 4.2: Alumina substrate intensity of the E field shown in dB scale, using fixed scale range, at 200 GHz, for the following lower boundary condition settings: a) perfect electrical conductor, b) radiation open (matching layer).

Guideline 2: *The worst case bound difference between the ideal (matching layer) and worst case (metal) boundary condition, extracted from the simulated response of the calibration structures, can be used to inform on the sensitivity of the calibration substrate to the real bounding condition employed.*

Characteristic impedance determination

To properly describe the behaviour of the transmission lines used during the calibration process in both TRL and Line-Reflect-Match (LRM) procedures the characteristic impedance of the line needs to be properly defined.

Guideline 3: *The following methods, among others, have been introduced in literature to properly account for the Z_0 of the line when radiation is present.*

- *Equation based modelling: In the model of Schnieder et al., IEEE Transactions on Microwave Theory and Techniques, January 2003, conductor backed coplanar waveguide with finite ground planes presenting dispersion and radiation properties are analyzed and modelled.*
- *Quasi-Analytical Tool: In van Berkel et al., IEEE Antennas and Propagation Magazine, June 2016, a software tool that allows for fast characterization of dynamic phenomena in a wide variety of transmission lines that include characteristic impedance, effective dielectric constant, and losses, such as radiation into space and surface waves is presented. The tool is available for free download on-line: <http://terahertz.tudelft.nl/Research/project.php?id=74&ti=27>*
- *3D EM FEM solver: In Galatro et al., IEEE Transactions on Microwave Theory and Techniques, April 2017, a procedure to use 3D EM commercially available tools is presented to properly extract the Z_0 of lines where radiation phenomena are present.*
- *In addition, when surface roughness, which also impacts the Z_0 computation, needs to be included the model described in Gold et al., IEEE Transactions on Microwave Theory and Techniques, Oct. 2017, can be employed.*

Structure optimisation for coplanar waveguides

In the CPW case, typical questions refer to design rules on how the width of the CPW ground planes and the ground-to-ground spacing should be chosen in order to keep parasitic mode excitation to a minimum. This has been investigated and the conclusion is given below.

Guideline 4: *The influence of CPW ground width and of ground-to-ground spacing, are contributing to parasitic effects in the calibrated results, in this case a dip in S-parameters at a certain frequency. Total CPW width determines the frequency where this dip occurs, and ground-to-ground spacing influences the strength of the dip behaviour. Thus, the best way to mitigate the impact of this dip is to keep the total CPW width smaller than the formula given in Schnieder et al. 2003, which requires a trade-off between the CPW total width, the used material and the upper frequency limit f_{max} .*

Chuck topology

The parasitic effects, due to the propagation of the substrate mode, are strongly dependent on the permittivity of the chuck material and the wafer. Figure 4.3 shows the vertical electric field component for the CPW line (20400 μm) on different chuck materials.

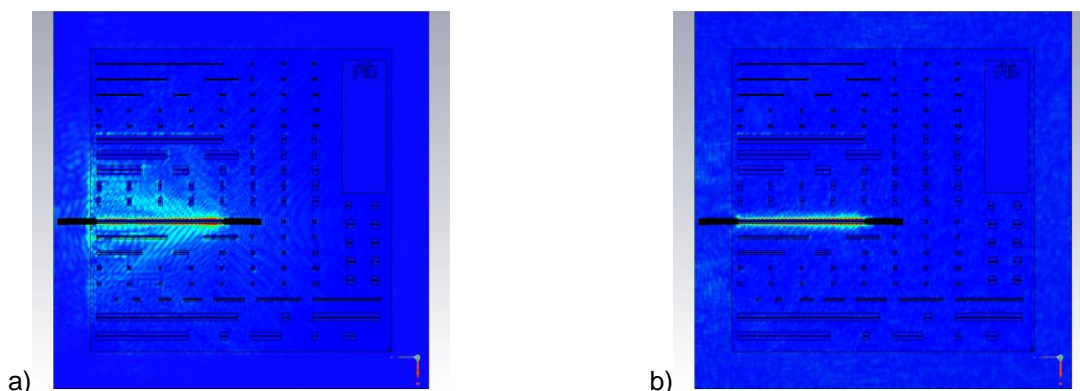


Figure 4.3: Field plots: magnitude of the electric field at 100 GHz (top view) excited with probe for nominal CPW ground width; a) on ceramic chuck $\epsilon_{r \text{ chuck}} = 6.0$; b) on chuck with same permittivity as the wafer, i.e., $\epsilon_{r \text{ chuck}} = 9.7$.

Guideline 5: Using for the chuck a material which has a permittivity value similar to the calibration substrate reduces the effects which contribute to the degradation of the accuracy of CPW mTRL calibrations. Further investigations have shown that this is true also for a chuck material with a permittivity larger than that of the wafer, because such a layered structure does not support surface waves either.

Impact of probe

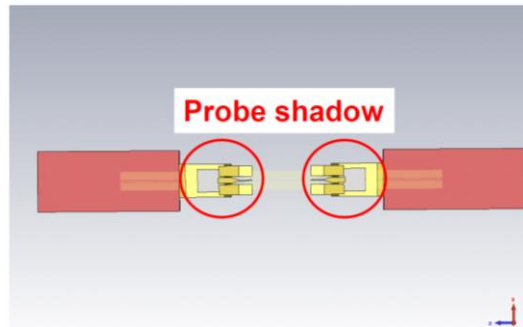


Figure 4.4: Design recommendations related to the probe construction.

Guideline 6: Simulation results indicate that one should keep sensitive regions of the probe shadow free of structures to avoid probe coupling to neighbouring structures, as shown in Figure 4.4 (investigations performed up to 70 GHz).

Thin-film micro-strip lines – coupling to adjacent elements

Thin-film micro-strip lines have also been investigated in this work. In order to perform the investigations, wafers with different layouts were designed and fabricated. What is studied here is the impact of positioning of the calibration structures and of the probe on the calibrated results of the different devices under test (DUTs). From the results above and further investigations on similar structures, design rules that help to reduce unintended side effects like coupling to neighbours or wafer and reticle edges have been developed.

Guideline 7: Basic layout conditions that should be fulfilled (extracted from the case of thin-film micro-strip to substrate separation of 18 μm thick).

(1) Place the calibration elements at sufficient distance

(2) Do not place structures within the probe shadow region below the probe (Figure 4.4 illustrates this). In contrast to the CPW case, the parasitic effects in a TFMSL environment are not related to substrate modes and crosstalk between structures, but only to coupling from the probe to the surrounding structures by fringing fields.

(3) For thin-film micro-strip lines as was the case for coplanar waveguides, one needs to keep the region of the probe shadow free of structures to avoid accuracy degradation.

Custom kits for LRM/TRL calibration

A custom calibration kit consisting of a full set of standards has been designed and fabricated to perform a TRL calibration in the back-end-of-line (BEOL) of the IHP 130 nm SiGe (silicon-germanium) BiCMOS process. Uniform grounded CPW lines have been considered. The fabricated chip microphotograph of the TRL kit is shown in Figure 4.5 (i.e., thru, reflect and line, respectively a, b and c).

The lines are implemented as grounded CPW, to reduce losses in the (semi) conductive substrate. All the structures employ aluminium pads, i.e., signal pad 30 x 50 μm^2 and larger grounds pads to allow different probe pitch to be used on the same structure (i.e., 75 μm and 100 μm). The thru line is a 200 μm long uniform coplanar waveguide (see Figure 4.5a). The calibration kit reflects are realized by two symmetric offset shorts (see Figure 4.5b), with an offset equal to half the thru length. This minimizes the distance between the centre of the thru and the location of the short, allowing to fix the sign of the square root solution in the TRL calibration (i.e., +/- open/short) for the entire calibration band. Note that when an electrical length of $\lambda/8$ is present the

sign needs to be changed to enforce phase continuity as shown in Figure 4.6, where the wanted behaviour is shown in red while the achieved one in blue. The error presented in the case where an electrical length is present between the centre of the thru and the short plane (Figure 4.6a) can be corrected using offset shorts as shown in Figure 4.6c.

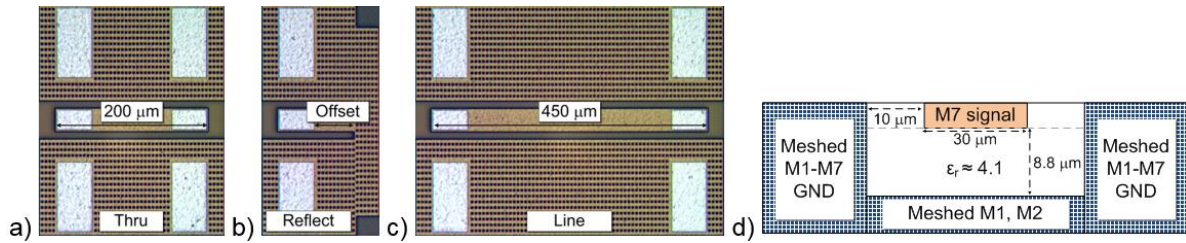


Figure 4.5: CPW calibration artefact realized on IHP SiGe 130 nm BiCMOS technology. (a) Microphotograph of the thru line, (b) of the reflect standard and (c) of the transmission line employed for the WR05 calibration kit. (d) Cross section sketch of the CPW line.

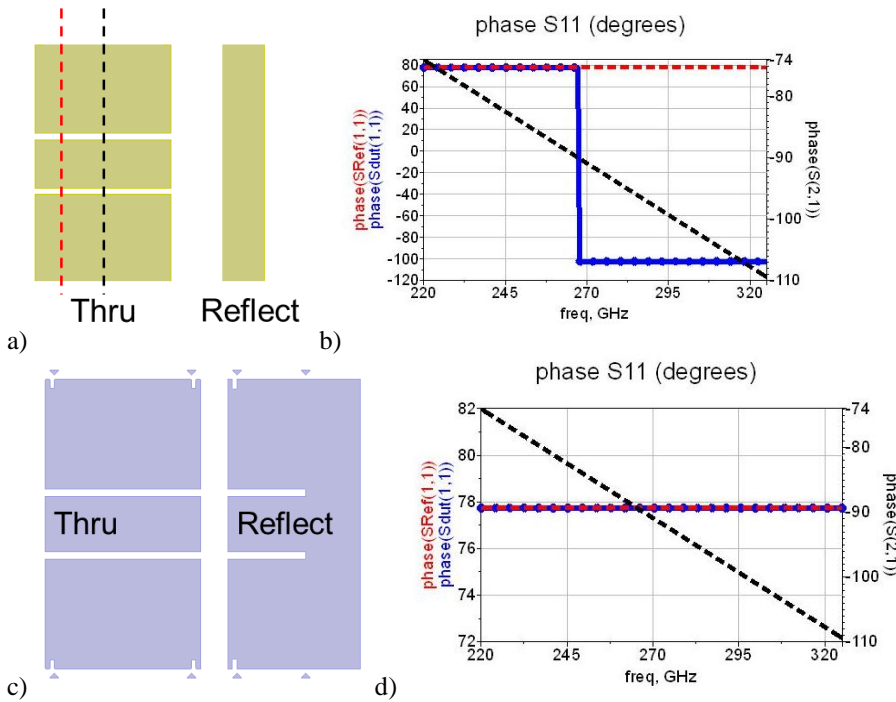


Figure 4.6: Layout and simulated response of flush (a-b) and offset short (c-d), showing the phase error that can occur when the electrical length between the centre of the thru and the intrinsic short location is larger than $\lambda/8$.

Guideline 8: When designing custom kits for LRM/TRL calibration the reflect should be realized as an offset one, keeping the minimum distance between the effective reflect and the center of the thru line (intrinsic calibration plane) to avoid requiring sign changes in the solution of the calibration equations.

Three transmission lines with lengths of 360, 450 and 680 μm are fabricated to allow single line TRL calibration in the WR3, WR5 and WR10 waveguide bands, respectively. Finally, a 600 μm long CPWG is used for calibration verification. The first two metal layers of the BEOL have been used to realize a meshed ground plane satisfying the metal density rules. The bottom ground plane is electrically connected to the coplanar ground planes using interleaved meshed metal on all layers and employing the maximum via density allowed. The CPW line is 30 μm wide and 3 μm thick with a 10 μm gap (see Figure 4.5c). The silicon dioxide acting as a dielectric has a relative permittivity of ca. 4.1, almost homogeneously among the entire structure, allowing simple simulation geometry.

The quality of the calibration achieved by the custom designed TRL kit, was benchmarked using the worst case bound metric using the 600 μm long CPWG as the verification structure. To normalize the S-parameter to the system impedance (i.e., 50 Ohm) one of the methods advised in guideline 3 (i.e., 3D EM FEM solver) and the calibration comparison method from D.F. Williams et al., IMS 1998, were employed. The result is shown in Figure 4.7.

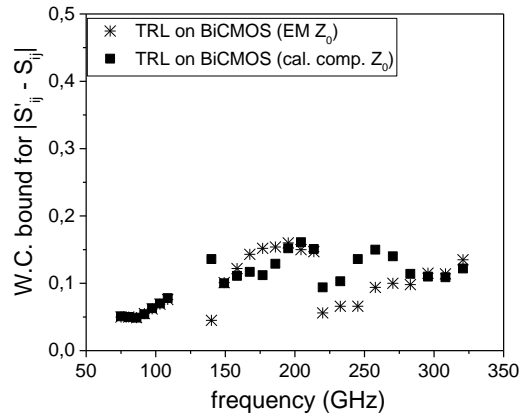


Figure 4.7: Comparison of probe-tips corrected measurements of a verification line manufactured on the SiGe BEOL in the frequency range 75-325 GHz.

4.5 Objective 5: Develop suitable calibration standards and methods for measurements of RF nano-devices

The objective 5 of the project addressed issues such as the impedance mismatch problems for calibrated S-parameters measurements of RF nano-devices and the challenge of probing at nanoscale dimensions. Conventional probing station and associated equipment for high frequency characterization in Micro and Nano electronics face several limitations in the case of nano-devices. One concerns the electrical mismatch while the impedance of high frequency measurement tools is low (close to 50 Ω) in front of the natural high impedance of nano-devices (higher than 10 k Ω). The second concerns the dimensional mismatch between probes and pads (several 100 μm) and the nano-device under test (several nm). These fundamental differences allow a lack of measurement accuracy decreasing for instance the modelling efficiency.

Impedance mismatch problems

This paragraph describes the solution to address the large mismatch between the VNA and nano-devices by utilizing RF-interferometer-based noise suppression techniques. The sensitivity degradation and larger trace noise in VNA measurements of non-50 Ω devices can be attributed, in a first approximation, to the presence of a scattered wave (i.e., **b**-wave) generated by the highly-mismatched device. Two techniques have been explored during the framework of the project to cancel the device generated **b**-wave by superimposing a second wave (**b_{int}**-wave), with opposite phase, effectively realizing an electrical high frequency interferometer.

For ultra low-noise and broadband measurements a new active RF interferometer approach is chosen in order not to be limited in performance and Γ_{dut} -range as for passive interferometers [2]. Figure 5.1(a) shows a sketch of the system for broadband measurements of extreme-impedance co-planar waveguide (CPW) devices designed at VSL. The interferometer generates a phase coherent **a_{int}**-wave using the **a₁** signal generated by the VNA. The entire interferometer is confined in the test path of the measurement system, as a single add-on module. The interferometer module is employed to cover the frequency range from 2 GHz up to 18 GHz. A Keysight PNA (5225A) is used for input reflection coefficient Γ measurements at a test-port power level of -5 dBm and IF-bandwidth of 30 Hz. At the output port of the interferometer, a GSG infinity probe with 150- μm pitch size is connected.

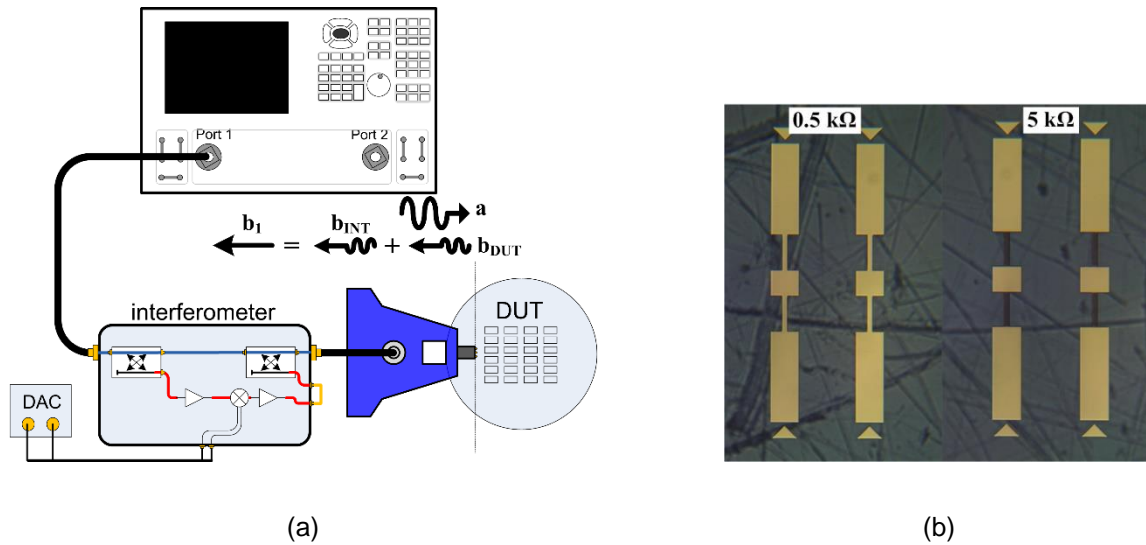
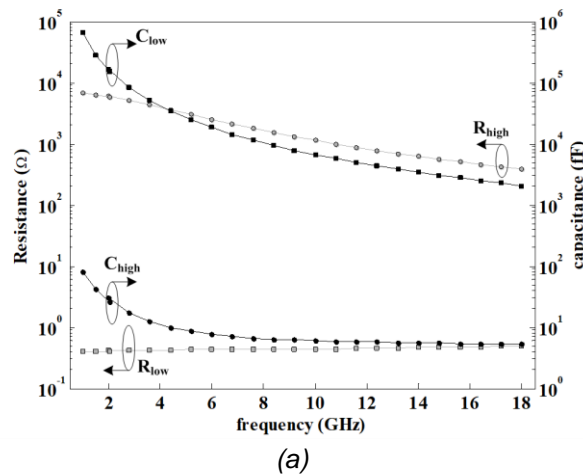


Figure 5.1: (a) Block diagram of the novel interferometer-based VNA for broadband measurement of highly-mismatched co-planar waveguide devices. (b) Photograph of 0.5-Ω and 5-kΩ CPW impedance standards manufactured on a fused-silica substrate, using a dedicated aluminum on titanium process developed at the Delft University of Technology.

A set of mismatched CPW impedance standards are manufactured to experimentally demonstrate the active noise suppression in highly-mismatched loading conditions. A photograph of both impedance standards is shown in Figure 5.1(b). The impedance standards are designed with nominal impedance of 0.5 Ω (Z_{low}) and 5 kΩ (Z_{high}). The VNA utilizes the novel interferometer to measure the S-parameters of both CPW impedance standards. To benchmark the interferometer-based VNA results to conventional VNA performance, the interferometer first is deactivated and the measurement system is calibrated using the well-known SOL technique utilizing a 50 Ω reference impedance, a short and an open standard. After completion of the calibration process, the Z_{low} and Z_{high} impedance standards are measured. The resistance R_{low} and R_{high} and the stray capacitance C_{low} and C_{high} corresponding to Z_{low} and Z_{high} standards are shown in Figure 5.2(a). In addition, a total of 101 sweeps are conducted to collect sufficient measurement values to estimate the corresponding noise values, see Figure 5.2(b) and Figure 5.2(c). Subsequently, both impedance standards are re-measured with the interferometer activated. The resulting noise values for R_{high} and C_{high} are shown in Figure 5.2 (b) and for R_{low} and C_{low} in Figure 5.2 (c) respectively for both the LF- and HF-interferometer. The Z_{low} results shown in Figure 5.2 (c) demonstrate marginal noise improvement of the interferometer-based VNA with respect to the conventional VNA. This likely is caused by the susceptibility of low-ohmic device measurements ($Z_{dut} < 1 \Omega$) to instabilities in contact resistance between the probe and DUT. In contrast, the Z_{high} results of Figure 5.2(b) demonstrate a significant noise improvement over the entire frequency range, ranging from a factor 8 at 1 GHz up to a factor 20 at 18 GHz.



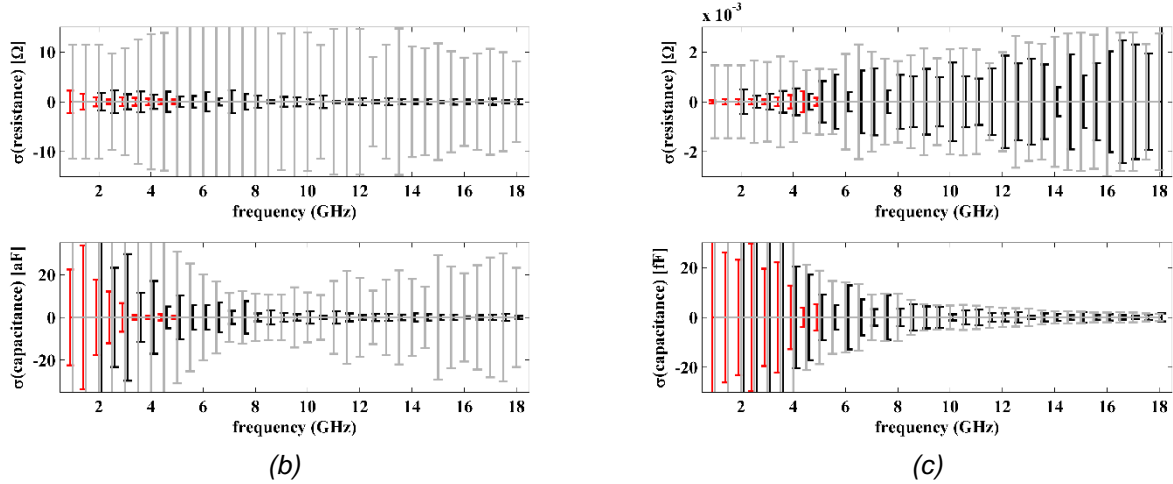


Figure 5.2: Measurement results of CPW Z_{low} and Z_{high} impedance standards in the 1-18 GHz frequency range. (a) Resistance R_{low} and R_{high} and stray capacitance C_{low} and C_{high} values corresponding to the Z_{low} and Z_{high} CPW standards. (b) and (c) show corresponding measurement noise values for the Z_{high} impedance standard and Z_{low} impedance standard respectively. Gray bars denote noise values measured with a conventional VNA; red and black bars depict noise values for a VNA with the novel LF- and HF-interferometer respectively.

Challenge of probing at nanoscale dimensions

This paragraph describes the solution to address the dimensional mismatch between conventional HF probing techniques and nano-devices by designing and fabricating a new type of MEMS based micrometer pitch miniaturized probes. A photography and SEM images of miniaturized probes are reported in Figure 5.3(a). The probe is realized on high resistivity 400 μm thick SOI substrate (1k Ωcm). The probe involves a 20 μm thick cantilever (400 μm of length). The mechanical properties in term of flexibility of this cantilever ensures the quality of the contact. The miniaturized CPW line is composed of a central gold conductor of 2 μm width and 500 nm thick with a 2.5 μm slot width. Such a probe is able to contact miniaturised pad of 3 x 3 μm^2 . Figure 5.3b shows a SEM image of a probe mounted in a PCB and a general view of the dedicated CalKit realized on GaAs substrate. The gain of area, compared to conventional probe CalKit, is close to two orders of magnitude (600 miniaturised CPW standards or test structures take the same place that 10 conventional ones).

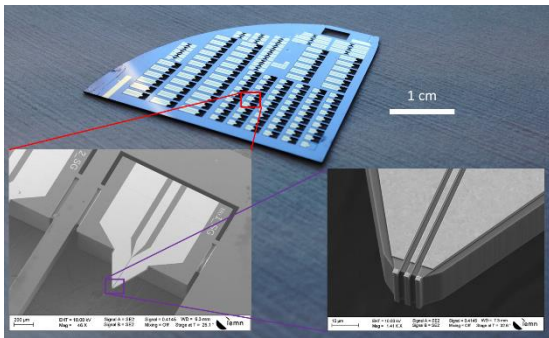


Figure 5.3(a). Image of quarter wafer with miniaturised micrometer pitch probes. SEM image of probe details.

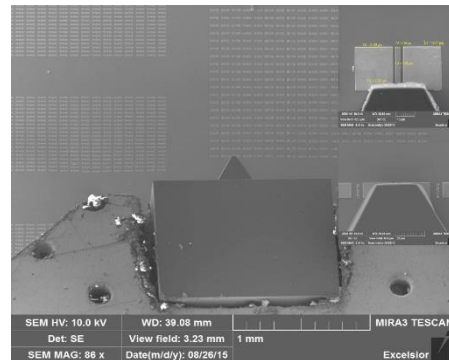


Figure 5.3(b). SEM images of probe mounted in a PCB above a miniaturised calKit.

These MEMS based probes are integrated in 254 μm thick duroid based PCB equipped with miniaturised SMP type 40GHz connector. The mounted probes are inserted in a unique instrument called ‘High frequency nanoprobe’ constituting of a SEM and piezoelectric based nano-positioners which was developed in the frame of French PIA EQUIPEX project (www.excelsior-ncc.eu). Some details of this nanoprobe is presented in Figure 5.4.

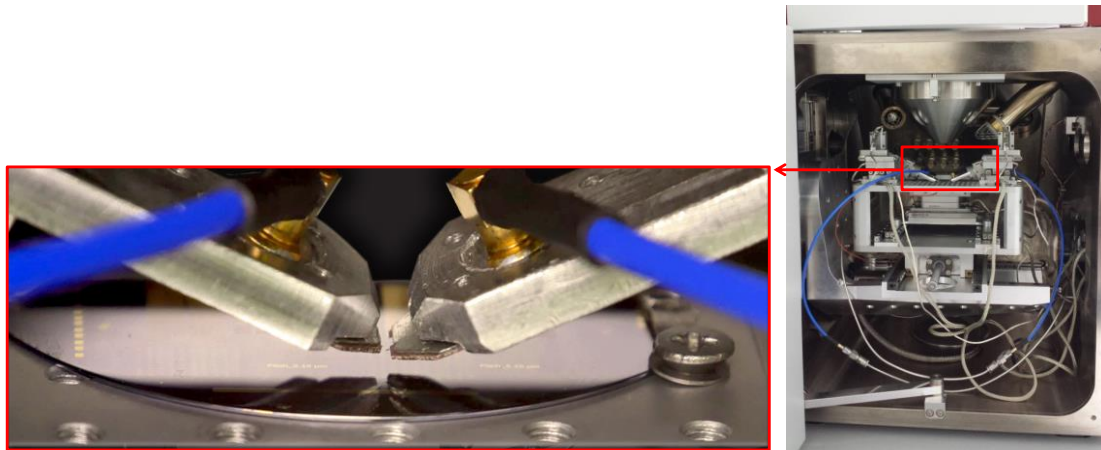


Figure 5.4: Images of the high frequency Nanoprober developed at IEMN (www.excelsior-ncc.eu).

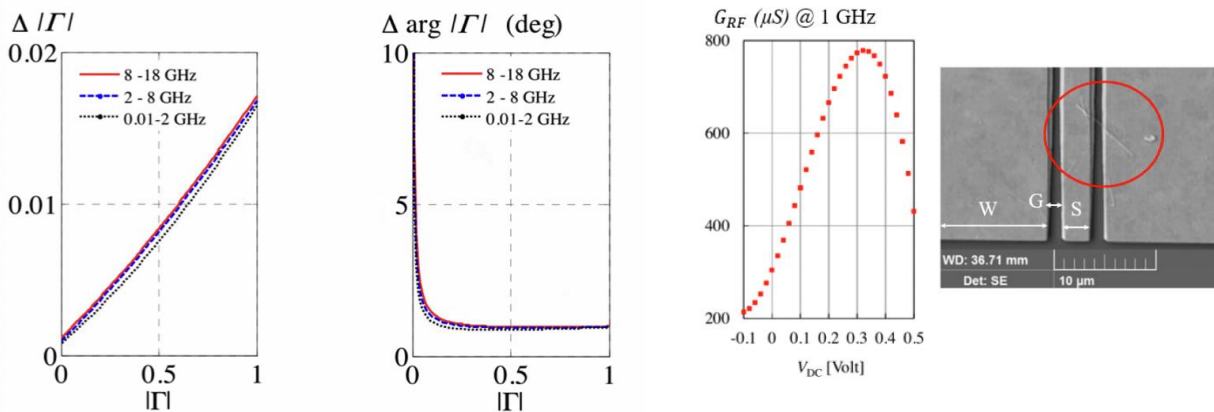


Figure 5.5 (a). Reflexion coefficient uncertainties up to 18GHz using miniaturised probes based on residual errors obtained by multiple SOL calibrations procedures.

Figure 5.5 (b). Right: SEM image of InAs nanowire inserted in miniaturised CPW test structure. Left: Conductance of InAs nanowire versus bias voltages deduced from one-port measurements at 1 GHz using miniaturised probes.

Proof of concept of such probes for microwave characterisation was achieved. As example, the uncertainty of one port measurement of reflexion coefficient is presented in Figure 5.5a. The uncertainties is fully similar to those obtained in best case by conventional on-wafer probing techniques and calibration methods. The gain of this nanoprober and associated miniaturised probes is mainly -the powerful integration of structures allowing a significant reduction of area devoted to the test and -the reduction of the influence of the test structure improving the efficiency of de-embedding procedure and increasing the accuracy of impedance measurement of nano-devices. For instance, the Figure 5.5b shows the GHz conductance of a unique Indium Arsenide (InAs) nanowire versus the bias conditions.

Access structures and extreme impedance standards

One of the main challenges was to design, fabricate and test a reference wafer that contained access structures and calibration standards that deal with the change in mechanical dimensions going from the microscale to the nanoscale, to enable reliable on-wafer metrology of nanoscale devices.

The reference wafer developed during this project included access structures suitable for conventional measurement systems, via a CPW that is tapered down to a few micrometres. The design of the access structures was based on a ground-signal-ground (GSG) CPW transmission line. For example, Figure 5.6(a) shows the dimensions of an open-circuit structure used as one of the calibration standards. Going from left to right in Figure 5.6(a), the signal conductor width is 100 μm and the separation between the signal and ground conductors is 66 μm. The signal and ground conductors are then tapered so that the signal conductor width is reduced to 4 μm. The same methodology can be extended to narrower lines, however the dimensions are limited by the uncertainty of the fabrication process. This provides a position where a nanoscale device can be placed and subsequently measured. The metal used for the conductor is gold of 500 nm thickness on a

400 μm gallium arsenide (GaAs) dielectric substrate. A 25 nm titanium layer was used beneath the gold to enhance adhesion to the substrate.

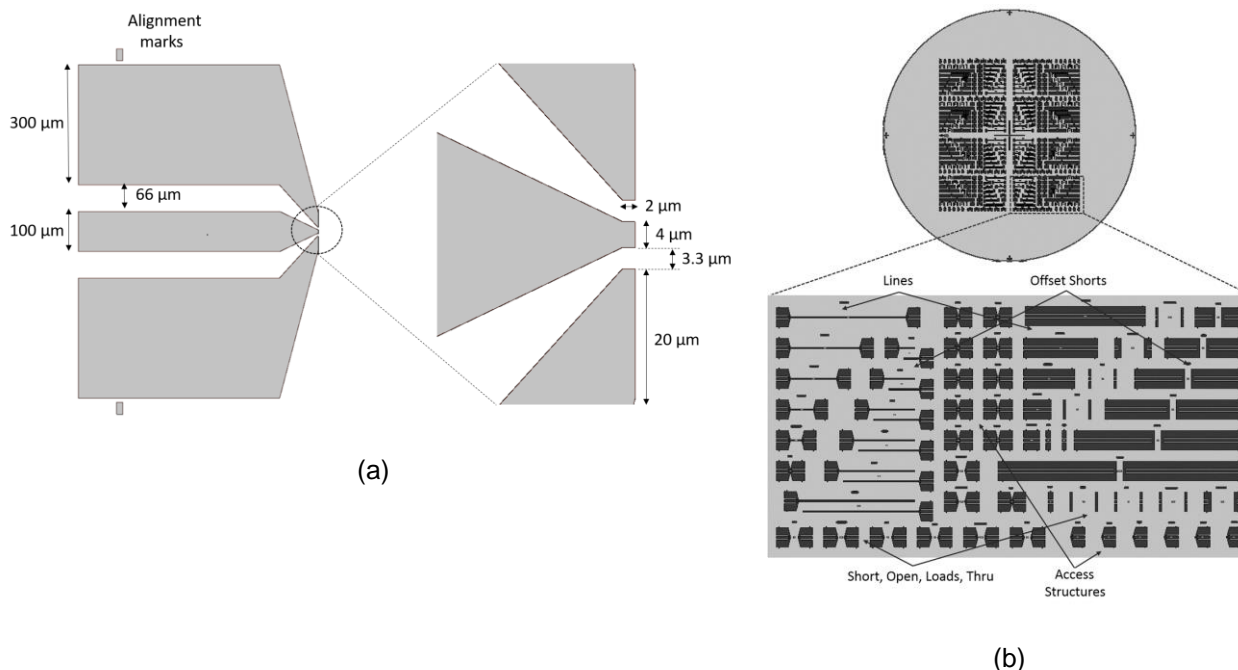


Figure 5.6: (a) Open-circuit calibration standard included on the reference wafer. The dimensions shown were selected to achieve a 50Ω characteristic impedance across the entire structure. (b) Layout of the fabricated 3 inch wafer including all the access structures and calibration standards

The dimensions of the CPW were chosen to preserve a 50Ω characteristic impedance (Z_0) at all places along the CPW line. This minimises reflections originating from the structures, and thus transfers the maximum amount of signal energy to the device under test (DUT). In addition, empty one-port and two-port structures with gaps between $2 \mu\text{m}$ and $20 \mu\text{m}$ are included to enable carbon nanotubes deposited on the wafer and subsequently measured. Figure 5.6(b) shows the 3inch wafer that was designed. It includes eight copies of the access structures and calibration standards. The reference wafer also included calibration standards that enable the reference planes for the measurements to be moved to the DUT. The standards enable several calibration techniques to be investigated for high-frequency characterisation at the nanoscale. The calibration standards included on the reference wafer were five lines having nominal lengths of 0.5 mm, 1 mm, 2 mm, 3 mm and 5 mm, five offset short-circuits with different phase delays, an open-circuit, a flush short-circuit, a 50Ω load, and a thru connection. Calibration standards were designed to enable a two-tier Vector Network Analyser (VNA) calibration to enable the reference planes for the measurements to be moved from the tips of the microwave probes to the end of the tapered conductor line of the CPW. The Si nanowires are grown by the vapour-liquid-solid (VLS) method from chemical vapour deposition (CVD) on a wafer substrate at IEMN in Lille. Figure 5.7 shows an electron microscopy image of the as-grown nanowires. The resulting nanowires are up to $20 \mu\text{m}$ long and have a diameter around 40 nm .

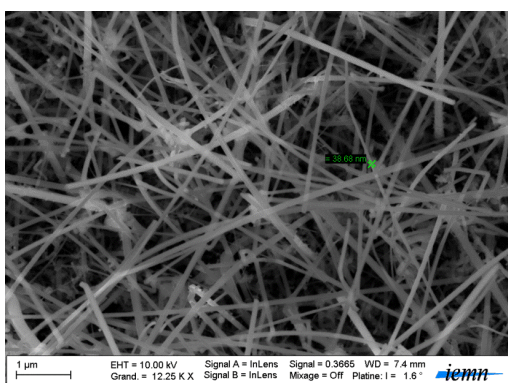


Figure 5.7: (a) Electron microscope image of a wafer with as-grown Si nanowires. (b) Optical image taken in the deposition process, showing in one-port access structure with 4 μm gap between inner and outer lines.

To deposit individual nanowires in the desired positions of the access structures an optical microscope equipped with hydraulic micromanipulators is used. The microscope is placed on an optical table reducing mechanical vibrations during the delicate process. The micromanipulators of the microscope are equipped with glass needles which have an apex radius of 1-2 μm and serve to pick up individual nanowires from the wafer. By scraping the wafer with the glass tip one or more nanowires are picked up and stick to the tip due to van-der-Waals forces. In case of multiple wires sticking to a tip, the second tip available can be used to isolate an individual one, as shown in Figure 5.7(a). Once an individual nanowire is located close to the tip's apex the glass needle is brought in coarse alignment close to the wafer hosting the access structures. In the following fine alignment, the nanowire is positioned in the orientation and place to connect signal and ground lines (one-port access structure) or to connect the gapped signal line (two-port access structure) as shown in Figure 5.7(b). In case the orientation or position are not ideal, or the nanowire does not detach from the carrying glass needle the second needle can be used to correct these shortcomings, which is also implicated in Figure 5.7(b) where the two used needles are in focus. Adhesion to the access structure is again provided by van-der-Waals forces and no additional electrical contacts are applied.

5 Impact

Key results of this project have been communicated to the end-users in industry and academia via training courses, workshops and publications at leading international microwave conferences. First standardisation efforts for on-wafer S-parameter measurements have been initiated at the recently founded On-Wafer Measurement User Forum, sponsored by the Automatic RF Techniques Group (ARFTG).

In particular, the following dissemination activities by the project have helped to strengthen the links to the end-user community:

- Two training courses, for end users: (i) "1st PlanarCal Training Course", at TU Delft, The Netherlands, in June 2016; (ii) "2nd PlanarCal Training Course", at METAS, Switzerland, in December 2017. All two courses involved project's partners as instructors and offered practical laboratory demonstrations.
- Two workshops at major international conferences, on: (i) "New developments in microwave measurements for planar circuits and components" at the International Microwave Symposium IMS2017, June 2017, (ii) "Modelling, Identification and Suppression of Parasitic Modes in On-Wafer Measurements" at the European Microwave Week EuMW2017, October 2017.
- 56 presentations at international scientific conferences and the publishing of 26 scientific papers, including three contributions to trade journals and professional press.
- Regular nine-monthly teleconferences with the Project's Advisory Board (PAB); a group of 6 international experts in the project's scientific areas.
- A project website (<https://planarcal.ptb.de/>) for end-users, and a LinkedIn Discussion Group.

Impact on industrial and other user communities

On-wafer microwave measurements play a key role in lowering the enormous costs of developing new products, because they enable industry to measure the true performance of RF components at the wafer level. Reliability and traceability of on-wafer measurements are vital for the entire RF and microwave industry, because they provide confidence in measurements and specifications. This is very important for customer/supplier relationships and where products need to be demonstrated as compliant to specifications or directives, regardless of who is doing the testing, or where the test is being done. The outcomes of this project will benefit all sectors of the electrical and electronics industries involved in characterisation and modelling of high-frequency devices and systems.

In particular, there have been four major achievements from which industry and the academic community can draw benefits.

As a world-wide first, this project demonstrated traceability for on-wafer S-parameter measurements of devices fabricated on fused silica and membrane technology substrates by establishing a comprehensive uncertainty budget. This traceability path can be applied to other configurations of measurement hardware, substrate materials and probes, as long as single-mode propagation is ensured.

Second, the specialised VNA measurement and uncertainty calculation software VNATools, developed by METAS, has been extended for on-wafer measurements and calibrations. The software package VNA Tools is available at no cost and can be downloaded from the METAS website (www.metas.ch/vnatools).

Third, guidelines for the design of calibration substrates have been developed, including the suppression of parasitic modes. They provide an overall framework on how to avoid effects such as parasitic modes and crosstalk through the substrate and between the microwave probes at millimetre wavelengths and beyond by formulating easy-to-follow design rules. Evidence of the efficacy of the design rules has been given through validated examples of calibration substrates fabricated during the lifetime of this project, and through measurements.

Fourth, Univ-Lille1 and VSL have developed a new generation of instrumentation aimed to address on-wafer measurement of nano-devices in the microwave regime. Future plans concern the RF test of high impedance CMOS devices from the silicon industry with targeted objectives such as improvement of the measurement accuracy and reduction of the wafer area dedicated to test and calibration.

Impact on the metrology and scientific communities

By the end of the project, new measurement capabilities have been established. These new measurement services are being provided subsequently to the stakeholder community and other industrial end-users in general. In the short-term, PTB will propose changes to the CMCs statements recorded in the BIPM key comparison database (KCDB) regarding planar S-parameter measurements up to 110 GHz. In the medium-term, the other NMIs participating in this project are also expected to propose changes to their CMCs statements. All these changes will account for the traceability routes for planar S-parameter measurements that have been newly developed within this project.

The extensions of the CPW model regarding high-frequency effects represent an indispensable tool for those working on advancing the state of the art, i.e. the metrological and scientific communities. Accurate modelling is not only essential for pushing the limits in circuit design but also to set up high-precision calibration routines and standardised measurements. The extended descriptions for transmission lines will also be communicated to the respective stakeholders providing circuit design CAD software.

The Best Practice Guide developed in this project represents a summary of state-of-the-art recommendations for performing on-wafer measurements together with a selection of the latest research results obtained over a period of three years during the PlanarCal project. Some of the uncertainties shown in the examples of this Guide can be significantly reduced by improving on the measurements of the wideband frequency-dependent material properties, which is a subject of future research.

As a result of this project the scientific communities in Europe will be enabled to expand their field of expertise compared to the international community and thus increase the chance of high level research and funded projects. Concerning the wider impact of the project, this can push technology development by accurate measurement results. These precise results will give new insight into technology processes and how to best optimise them.

Impact on relevant standards

Up to now, no documentary standards existed for on-wafer calibrations and measurements. To change this situation, during this project, the consortium has engaged with the ARFTG Board of Directors, and an On-wafer Users' Forum has been set up. This Forum has met during several major international conferences. Also, a pre-standardisation Special Interest Group (SIG) for on-wafer measurements has been set up. This SIG has developed a draft Project Authorisation Request (PAR) which is required as part of the process for initiating an IEEE standards-making activity. The draft PAR has been submitted to the IEEE Standards Association shortly after the end of the project.

Longer-term economic, social and environmental impacts

The results of this project will enable manufacturers of planar microwave circuits and components to offer assured products with defensible specifications which are supported for the first time through on-wafer measurement traceability chains. By fulfilling cost and quality assurance requirements more easily, this project will help products in different areas to become market leaders. These markets include consumer electronics, security and detection systems, medical diagnostics, climate change monitoring, and the entire telecommunications and automotive industry. The outcomes of this project will benefit all sectors of the electrical and electronics industries involved in characterisation and modelling of high-frequency devices and

systems. Increasing technological innovation will help secure existing jobs and create future jobs in Europe as a location for business.

As wireless data communications are becoming more and more commonplace, the average electromagnetic radiation intensity is steadily increasing. It is therefore very important to decrease the transmitted power of radio-communication systems. The development of characterisation and measurement methods for planar circuits and components as carried out in this project will help to increase the efficiency of mobile communication systems, and thus to reduce the overall electromagnetic radiation.

Examples of user uptake

The project successfully increased the level of confidence for industrial S-parameter measurements of planar microwave devices and components, including emerging nanotechnology devices. In addition the improved measurement capabilities and the design and validation of new methods and technologies provide opportunities for instrumentation manufacturers to develop innovative solutions to meet the electronic industry's current and future needs.

The project has had a number of uptakes:

- METAS has enhanced the VNATools software package with on-wafer capabilities, allowing for the calculation of uncertainties. During the lifetime of the project more than 430 new users have registered worldwide and the community is growing steadily.
- PTB has extended the calibration capabilities to include traceable planar S-parameter measurements on selected substrates up to 110 GHz.
- With support from PTB, R&S designed and fabricated a PCB calibration substrate suitable for frequencies between 50 and 110 GHz. In the corresponding uncertainty budget, the new CPW model including surface roughness was utilised and helped in understanding the major sources of uncertainty observed in the measurements.
- Univ-Lille1 has solved metrological issues related to the electrical characterization of nanoelectronic devices in a collaboration with STMicroelectronics, one of the leading semiconductor companies in Europe. Univ-Lille1 together with STMicroelectronics assessed the traceability of sub-fF varactors at the industrial level, addressing RF tuning optimization within multi-bands wireless devices applications. The method used should be of interest to the entire semiconductor and telecommunication industry.
- With the aid of PTB and FVB, RF360 has designed, simulated and fabricated calibration structures on piezoelectric substrates which allowed exploring differences between measurements performed with ground-signal-ground and ground-signal probes.
- The Gradient Model of FAU, describing the interaction of electromagnetic fields with rough surfaces, was implemented in the leading 3D EM simulation software CST Microwave Studio and is now publicly available.
- Several invitations have been extended to consortium members and the project coordinator to present the project's outcomes at international workshops and meetings of the ARFTG User Forum and the IEEE MTT-11 committee, respectively.
- The work performed in this project will serve as a basis for extending traceability to frequencies beyond 110 GHz in a follow-on EMPIR project, TEMMT. TEMMT will benefit not only from the fundamental work on traceability and design guidelines performed in PlanarCal, but also from the experiences gained in measurement intercomparisons at D-band (110-170 GHz) and G-band (140-220 GHz).
- Anritsu, R&S and Keysight had components and test equipment included in the investigations in the project. Setting up the uncertainty budgets required a thorough characterization of their systems, in particular of their VNAs. This has effectively benchmarked the performance of the VNAs and provides useful, independent, evaluation of these components and equipment within the context of this project.
- PTB is now evaluating the introduction of a customer calibration service for planar S-parameter measurements up to 110 GHz for selected substrate and probe combinations based on the work achieved in this project. At the present time, there are no other NMIs offering such a service.
-

6 List of publications

- [1] F. Mubarak, R. Romano, and M. Spirito, "Evaluation and modeling of measurement resolution of a vector network analyzer for extreme impedance measurements," in 86th ARFTG Microwave Measurement Conference, 2015. [Online]. Available: <http://ieeexplore.ieee.org/document/7381475/?arnumber=7381475&tag=1>
- [2] M. Bieler and U. Arz, "Characterization of high-frequency interconnects: Comparison between time- and frequency-domain methods," in 20th IEEE Workshop on Signal and Power Integrity (SPI), 2016. [Online]. Available: <https://oar.ptb.de/resources/show/10.7795/EMPIR.14IND02.CA.20190403D>
- [3] K. Daffé, G. Dambrine, F. von Kleist-Retzow, and K. Haddadi, "RF wafer probing with improved contact repeatability using nanometer positioning," in 87th ARFTG Microwave Measurement Conference, 2016. [Online]. Available: <https://hal.archives-ouvertes.fr/hal-02083251>
- [4] M. Bieler and U. Arz, "Comparison between time- and frequency-domain high-frequency device characterizations," in Conference on Precision Electromagnetic Measurements (CPEM), 2016. [Online]. Available: <https://oar.ptb.de/resources/show/10.7795/EMPIR.14IND02.CA.20190403E>
- [5] G. Gold and K. Helmreich, "Modeling of transmission lines with multiple coated conductors," in 46th European Microwave Conference (EuMC), 2016, pp. 635–638. [Online]. Available: <http://dx.doi.org/10.1109/EuMC.2016.7824423>
- [6] H. Votsi et al., "Development of a reference wafer for on-wafer testing of extreme impedance devices," in 88th ARFTG Microwave Measurement Conference, 2016. [Online]. Available: <http://dx.doi.org/10.1109/ARFTG.2016.7839719>
- [7] L. Galatro and M. Spirito, "Millimeter-Wave On-Wafer TRL Calibration Employing 3-D EM Simulation-Based Characteristic Impedance Extraction," IEEE Transactions on Microwave Theory and Techniques, vol. 65, no. 4, pp. 1315–1323, Apr. 2017. [Online]. Available: <https://ieeexplore.ieee.org/stamp/stamp.jsp?tp=&arnumber=7837598>
- [8] F. J. Schmückle, T. Probst, U. Arz, G. N. Phung, R. Doerner, and W. Heinrich, "Mutual interference in calibration line configurations," in 89th ARFTG Microwave Measurement Conference, 2017. [Online]. Available: <https://www.fbh-berlin.com/publications-patents/publications/title/mutual-interference-in-calibration-line-configurations>
- [9] M. Wollensack, J. Hoffmann, D. Stalder, J. Rufenacht, and M. Zeier, "VNA tools II: Calibrations involving eigenvalue problems," in 89th ARFTG Microwave Measurement Conference, 2017. [Online]. Available: <https://oar.ptb.de/resources/show/10.7795/EMPIR.14IND02.CA.20190404>
- [10] G. N. Phung, F. J. Schmückle, R. Doerner, T. Fritzsche, and W. Heinrich, "Impact of parasitic coupling on multilayer TRL calibration," in 47th European Microwave Conference (EuMC), 2017, pp. 835–838. [Online]. Available: <https://www.fbh-berlin.com/publications-patents/publications/title/impact-of-parasitic-coupling-on-multilayer-trl-calibration-1>
- [11] K. Daffé et al., "Nano-probing station incorporating MEMS probes for 1D device RF on-wafer characterization," in 47th European Microwave Conference (EuMC), 2017, pp. 831–834. [Online]. Available: <https://hal.archives-ouvertes.fr/hal-01726555>
- [12] N. Ridler, R. Clarke, and M. Salter, "Mind the Gap". Establishing Measurement Capability in the Terahertz Gap Region - from 0.1 THz to 1.1 THz," ARMMS Conference Digest. ARMMS, Nov. 2017. [Online]. Available: <http://eprints.whiterose.ac.uk/125335/>
- [13] R. Clarke, C. Li, and N. Ridler, "An Intra-Laboratory Investigation of On-wafer Measurement Reproducibility at Millimeter-wave Frequencies," 90th ARFTG Microwave Measurement Conference, 2017. [Online]. Available: <http://eprints.whiterose.ac.uk/125336/>
- [14] T. Probst, R. Dörner, M. Ohlrogge, R. Lozar, and U. Arz, "110 GHz On-Wafer Measurement Comparison on Alumina Substrate," in 90th ARFTG Microwave Measurement Conference, 2017. [Online]. Available: <https://oar.ptb.de/resources/show/10.7795/EMPIR.14IND02.CA.20190403A>
- [15] U. Arz, S. Zinal, T. Probst, G. Hechtischer, F.-J. Schmückle, and W. Heinrich, "Establishing Traceability for On-Wafer S-Parameter Measurements of Membrane Technology Devices up to 110 GHz," 90th ARFTG Microwave Measurement Conference, 2017. [Online]. Available: <https://oar.ptb.de/resources/show/10.7795/EMPIR.14IND02.CA.20190403> (*Best Paper Award*)

- [16] G. N. Phung, F.-J. Schmückle, R. Doerner, W. Heinrich, T. Probst, U. Arz, "Effects degrading accuracy of CPW mTRL calibration at W-band," Proceedings of International Microwave Symposium (IMS), 2018, pp. 1296-1299. [Online]. Available: <https://www.fbh-berlin.com/publications-patents/publications/title/effects-degrading-accuracy-of-cpw-mtrl-calibration-at-w-band>
- [17] T. Probst, S. Zinal, R. Doerner, and U. Arz, "On the Importance of Calibration Standards Definitions for On-Wafer Measurements up to 110 GHz," in 91st ARFTG Microwave Measurement Conference, 2018. [Online]. Available: <https://oar.ptb.de/resources/show/10.7795/EMPIR.14IND02.CA.20190403C>
- [18] F. Mubarak, V. Mascolo, G. Rietveld, M. Spirito, K. Daffe, and K Haddadi, "Parameterization Models for Traceable Characterization of Planar CPW SOL Calibration Standards," Conference on Precision Electromagnetic Measurements (CPEM), 2018. [Online]. Available: <https://hal.archives-ouvertes.fr/hal-02085776>
- [19] K. Haddadi, P. Polodolov, D. Theron, and G. Dambrine, "Quantitative error analysis in near-field scanning microwave microscopy," in 3rd International Conference on Manipulation, Automation and Robotics at Small Scales, MARSS 2018, Nagoya, Japan, 2018. [Online]. Available: <https://hal.archives-ouvertes.fr/hal-01913677>
- [20] K. Haddadi et al, "On-Wafer Series-Through Broadband Measurement of Sub-ff55-nm MOS RF Voltage-Tunable Capacitors," IEEE Microwave and Wireless Components Letters, 2018, vol 28, no 9, p. 831-833. [Online]. Available: <https://hal.archives-ouvertes.fr/hal-01873048>
- [21] C. Liu, A. Wu, C. Li, and N. Ridler, "A New SOLT Calibration Method for Leaky On-Wafer Measurements Using a 10-Term Error Model," IEEE Transactions on Microwave Theory and Techniques, vol. 66, no. 8, pp. 3894–3900, Aug. 2018. [Online]. Available: <http://dx.doi.org/10.1109/TMTT.2018.2832052>
- [22] G. N. Phung, F.-J. Schmückle, R. Doerner, W. Heinrich, T. Probst, U. Arz, "Impact of Substrate Modes on mTRL-Calibrated CPW Measurements in G Band," 48th European Microwave Conference (EuMC), 2018. [Online]. Available: https://www.fbh-berlin.com/fileadmin/downloads/Publications/2018/2018_06_04_EuMC_2018_Mode_Suppression_final_03.pdf
- [23] K. Daffé, F. Mubarak, V. Mascolo, H. Votsi, N. Ridler, G. Dambrine, I. Roch, K. Haddadi, "On-wafer broadband microwave measurement of high impedance devices - CPW test structures with integrated metallic nano-resistances," 48th European Microwave Conference (EuMC), 2018.[Online]. Available: <https://hal.archives-ouvertes.fr/hal-02056825>
- [24] U. Arz, A. Savin, "On-wafer residual error correction through adaptive filtering of verification line measurements," CEMi'18 International Workshop on Computing, Electromagnetics, and Machine Intelligence, 2018. [Online]. Available: <https://oar.ptb.de/resources/show/10.7795/EMPIR.14IND02.CA.20190403F>
- [25] F. A. Mubarak, R. Romano, L. Galatro, V. Mascolo, G. Rietveld, and M. Spirito, "Noise Behavior and Implementation of Interferometer Based Broadband VNA," IEEE Transactions on Microwave Theory and Techniques, vol. 67, nr. 1, pp. 249-260, Jan. 2019. <http://dx.doi.org/10.1109/TMTT.2018.2874667> [Online]. Available: <https://ieeexplore.ieee.org/stamp/stamp.jsp?tp=&arnumber=8566175>
- [26] G.N. Phung, F.-J. Schmückle, R. Doerner, T. Fritsch, S. Schulz and W. Heinrich, "Crosstalk Effects of Differential Thin-Film Microstrip Lines in Multilayer Motherboards", Proc. of the 12th German Microwave Conference, pp. 178-181, Mar. 2019. [Online]. Available: https://www.fbh-berlin.com/fileadmin/downloads/Publications/2019/2019_02_20_GeMiC_GNP_repository.pdf
- [27] G.N. Phung, F.-J. Schmückle, R. Doerner, B. Kähne, T. Fritsch, U. Arz and W. Heinrich, "Influence of Microwave Probes on Calibrated On-Wafer Measurements," IEEE Transactions on Microwave Theory and Techniques, vol. 67, nr. 5, pp. 1892-1900, May 2019. [Online]. Available: https://www.fbh-berlin.de/fileadmin/downloads/Publications/2019/FINAL_VERSION_repository.pdf
- [28] U. Arz, K. Kuhlmann, T. Dziomba, G. Hechtfisher, G.N. Phung, F.J. Schmückle and W. Heinrich, "Traceable Coplanar Waveguide Calibrations on Fused Silica Substrates up to 110 GHz," accepted for publication in IEEE Transactions on Microwave Theory and Techniques, 2019. [Online]. Available: <http://dx.doi.org/10.1109/TMTT.2019.2908857>

- [29] U. Arz, T. Probst, K. Kuhlmann, N. Ridler, X. Shang, F. Mubarak, J. Hoffmann, M. Wollensack, M. Zeier, G. N. Phung, W. Heinrich, K. Lomakin, G. Gold, K. Helmreich, R. Lozar, G. Dambrine, K. Haddadi, M. Spirito, R. Clarke, "Best Practice Guide for Planar S-Parameter Measurements using Vector Network Analysers," [Online]. Available: <https://oar.ptb.de/resources/show/10.7795/530.20190424B>
- [30] M. Spirito, U. Arz, G. N. Phung, F. J. Schmückle, W. Heinrich, R. Lozar "Guidelines for the design of calibration substrates, including the suppression of parasitic modes for frequencies up to and including 325 GHz," [Online]. Available: <https://oar.ptb.de/resources/show/10.7795/530.20190424A>

7 Contact details

The public web-site for this project is <https://planarcal.ptb.de>

The contact person for general enquiries is Dr. Uwe Arz, PTB (uwe.arz@ptb.de).